Article

Cell Reports

Class IIa Histone Deacetylases Drive Toll-like Receptor-Inducible Glycolysis and Macrophage Inflammatory Responses via Pyruvate Kinase M2

Graphical Abstract

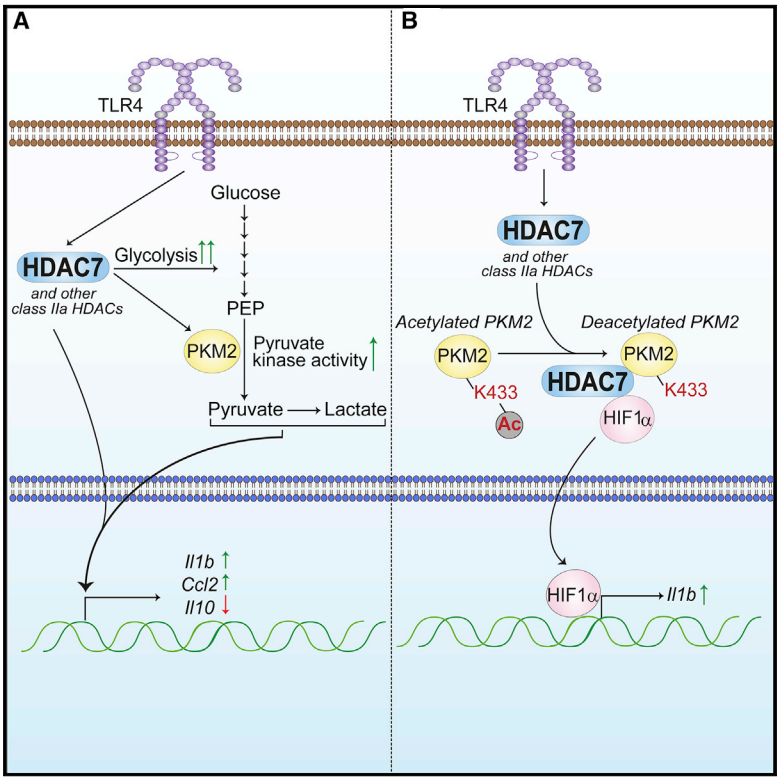

Highlights

- The class IIa HDAC, HDAC7, drives TLR4-inducible glycolysis in macrophages
- An interaction between HDAC7 and PKM2 drives macrophage immunometabolic responses
- Deacetylation of PKM2 at K433 licenses it to drive proinflammatory IL-1β expression
- Multiple class IIa HDACs can engage the PKM2 immunometabolic signaling hub

Authors

Kaustav Das Gupta, Melanie R. Shakespear, James E.B. Curson, ..., Jennifer L. Stow, David P. Fairlie, Matthew J. Sweet

Correspondence

m.sweet@imb.uq.edu.au

In Brief

Das Gupta et al. show that HDAC7 and other class IIa HDAC enzymes control macrophage metabolism. They initiate TLR-inducible glycolysis in these cells and interact with the glycolytic enzyme PKM2 to drive inflammatory responses *in vitro* and *in vivo*. Class IIa HDAC inhibitors may have potential for attenuating immunometabolism-linked inflammation.

Das Gupta et al., 2020, Cell Reports *30*, 2712–2728
February 25, 2020
https://doi.org/10.1016/j.celrep.2020.02.007

CellPress

OPEN ACCESS
CellPress

Cell Reports
Article

Class IIa Histone Deacetylases Drive Toll-like Receptor-Inducible Glycolysis and Macrophage Inflammatory Responses via Pyruvate Kinase M2

Kaustav Das Gupta,[1,2,10] Melanie R. Shakespear,[1,2,10] James E.B. Curson,[1,2] Ambika M.V. Murthy,[1,2] Abishek Iyer,[1,2,3] Mark P. Hodson,[4,5,6] Divya Ramnath,[1,2] Vikas A. Tillu,[1] Jessica B. von Pein,[1,2] Robert C. Reid,[1,2,3] Kathryn Tunny,[1] Daniel M. Hohenhaus,[1] Shayli Varasteh Moradi,[7] Gregory M. Kelly,[1] Takumi Kobayashi,[8] Jennifer H. Gunter,[9] Alexander J. Stevenson,[1] Weijun Xu,[1,2,3] Lin Luo,[1,2] Alun Jones,[1] Wayne A. Johnston,[7] Antje Blumenthal,[8] Kirill Alexandrov,[7] Brett M. Collins,[1] Jennifer L. Stow,[1,2] David P. Fairlie,[1,2,3] and Matthew J. Sweet[1,2,11,*]

[1]Institute for Molecular Bioscience (IMB), The University of Queensland, Brisbane, Queensland 4072, Australia
[2]IMB Centre for Inflammation and Disease Research and Australian Infectious Diseases Research Centre, The University of Queensland, Brisbane, Queensland 4072, Australia
[3]ARC Centre of Excellence in Advanced Molecular Imaging, IMB, The University of Queensland, Brisbane, Queensland 4072, Australia
[4]School of Pharmacy, The University of Queensland, Brisbane, Queensland 4072, Australia
[5]Metabolomics Australia, Australian Institute for Bioengineering and Nanotechnology, The University of Queensland, Brisbane, Queensland 4072, Australia
[6]Victor Chang Cardiac Research Institute, Sydney, New South Wales 2010, Australia
[7]CSIRO-QUT Synthetic Biology Alliance, Centre for Tropical Crops and Biocommodities, Queensland University of Technology (QUT), Gardens Point Campus, Brisbane, Queensland 4000, Australia
[8]The University of Queensland Diamantina Institute, The University of Queensland, Brisbane, Queensland 4072, Australia
[9]Australian Prostate Cancer Research Centre-Queensland, Institute of Health and Biomedical Innovation, School of Biomedical Sciences, Faculty of Health, Translational Research Institute, Queensland University of Technology (QUT), Brisbane, Queensland 4102, Australia
[10]These authors contributed equally
[11]Lead Contact
*Correspondence: m.sweet@imb.uq.edu.au
https://doi.org/10.1016/j.celrep.2020.02.007

SUMMARY

Histone deacetylases (HDACs) drive innate immune cell-mediated inflammation. Here we identify class IIa HDACs as key molecular links between Toll-like receptor (TLR)-inducible aerobic glycolysis and macrophage inflammatory responses. A proteomic screen identified the glycolytic enzyme pyruvate kinase M isoform 2 (Pkm2) as a partner of proinflammatory Hdac7 in murine macrophages. Myeloid-specific Hdac7 overexpression in transgenic mice amplifies lipopolysaccharide (LPS)-inducible lactate and promotes a glycolysis-associated inflammatory signature. Conversely, pharmacological or genetic targeting of Hdac7 and other class IIa HDACs attenuates LPS-inducible glycolysis and accompanying inflammatory responses in macrophages. We show that an Hdac7-Pkm2 complex acts as an immunometabolism signaling hub, whereby Pkm2 deacetylation at lysine 433 licenses its proinflammatory functions. Disrupting this complex suppresses inflammatory responses *in vitro* and *in vivo*. Class IIa HDACs are thus pivotal intermediates connecting TLR-inducible glycolysis to inflammation via Pkm2.

INTRODUCTION

Innate immune cells use pattern recognition receptors to respond to exogenous and endogenous danger signals (Zhang and Mosser, 2008). Widely studied in this context are the Toll-like receptors (TLRs), which use a signaling framework consisting of Toll/interleukin (IL)-1 receptor-containing adaptor proteins, serine/threonine kinases, tyrosine kinases, and ubiquitin-modifying enzymes to initiate activation of proinflammatory transcription factors such as NF-κB (Rossol et al., 2011; O'Neill et al., 2013). Regulated lysine acetylation has also emerged as an important post-translational modification controlling TLR signaling responses (Rossol et al., 2011; Shakespear et al., 2011).

Lysine acetylation is controlled by the opposing actions of two enzyme families, histone acetyltransferases and histone deacetylases (HDACs). Histones were the first identified targets of HDACs (Allfrey et al., 1964), but numerous non-histone substrates have since been discovered (Choudhary et al., 2009). Of the classical zinc-dependent HDACs (HDAC1–11), class IIa (HDAC4, 5, 7, and 9) enzymes are expressed in a tissue-restricted manner and are defined by a highly homologous C-terminal deacetylase domain, an N-terminal protein interaction domain, and nuclear export and import signals. These enzymes can act as transcriptional derepressors through signal-induced nuclear export (Martin et al., 2007; Schlumm et al., 2013), but some signals can also promote their nuclear

translocation for gene activation (Martin et al., 2007; Mihaylova et al., 2011).

Broad-spectrum inhibitors of classical HDACs (HDACi) can suppress or amplify the TLR-inducible production of different inflammatory mediators from macrophages and other innate immune cells (Aung et al., 2006; Brogdon et al., 2007; Roger et al., 2011). Moreover, selective targeting of distinct HDAC classes and isozymes in macrophages differentially affected such responses (Halili et al., 2010), suggesting that specific HDACs can have either pro- or anti-inflammatory functions in a single cell type. For example, class I HDACs limit TLR-induced inflammation by transcription factor deacetylation (Ashburner et al., 2001; Sadler et al., 2015), while class II HDACs can promote macrophage inflammatory responses (Shakespear et al., 2013; Yan et al., 2014; Youn et al., 2016). In addition to their anti-cancer properties (Falkenberg and Johnstone, 2014), several broad-spectrum HDACi were efficacious in animal models of inflammatory diseases (Shakespear et al., 2011). Multiple mechanisms likely contribute to these effects, including suppression of innate immune cell activation and enhancement of T regulatory cell functions (Shakespear et al., 2011; Falkenberg and Johnstone, 2014; Das Gupta et al., 2016).

Recent studies have demonstrated that inflammatory outputs of macrophages are intimately linked to their metabolic status (Das Gupta et al., 2016; O'Neill and Pearce, 2016). TLR activation causes a marked increase in aerobic glycolysis and a disrupted tricarboxylic acid (TCA) cycle to drive specific proinflammatory responses (Gaber et al., 2017). A key component of the metabolic shift in activated macrophages is the glycolytic enzyme pyruvate kinase M (PKM), which exists in two alternatively spliced isoforms (PKM1 and PKM2) (Takenaka et al., 1991). Whereas PKM1 catalyzes the final step of glycolysis, converting phosphoenolpyruvate to pyruvate, PKM2 also promotes the expression of glycolytic and inflammatory genes (Alves-Filho and Pålsson-McDermott, 2016). However, the molecular components required for PKM2-dependent inflammatory functions are not well understood. Here we report that, through their capacity to regulate the function of the glycolytic enzyme PKM2, class IIa HDACs, particularly HDAC7, provide a molecular link between TLR-inducible aerobic glycolysis and inflammatory responses in macrophages. Moreover, we demonstrate that selective inhibition of class IIa HDACs can attenuate glycolysis-fueled inflammatory responses in macrophages both *in vitro* and *in vivo*. In so doing, we define a pharmacologically targetable pathway that drives immunometabolism-linked inflammation in the innate immune system.

RESULTS

Hdac7 Drives Selective Inflammatory Responses in Macrophages

To investigate mechanisms by which class IIa HDACs drive inflammation, we focused on Hdac7, which promotes TLR-inducible proinflammatory responses in murine macrophages (Shakespear et al., 2013). We first used a binary MacBlue/UAS-GAL4 system for myeloid-specific transgenics (Ovchinnikov et al., 2008) to generate mice expressing V5-tagged Hdac7-u (Margariti et al., 2010) in the myeloid compartment. We previously showed a selective role for this Hdac7 variant, which lacks the first 22 amino acids and cannot bind to the transcriptional repressor Ctbp, in promoting inflammatory responses in RAW 264.7 murine macrophage-like cells (Shakespear et al., 2013). The MacBlue mouse line was crossbred with a second transgenic mouse line containing Hdac7-V5 under the control of a GAL4-responsive promoter. Only offspring inheriting both transgenes (Mac-Hdac7 mice; Figure 1A, left) express ectopic Hdac7-V5 in primary macrophages (Figure 1A, right). Bone marrow-derived macrophages (BMMs) from Mac-Hdac7 mice showed increased LPS-induced levels of *Il12b* mRNA and secreted Il12b (Il-12p40) protein (Figures 1B and S1A), consistent with our previous findings in RAW 264.7 cells (Shakespear et al., 2013). This effect was selective; LPS-induced *Nos2* mRNA expression and the subsequent generation of nitric oxide (NO) were unaffected in Mac-Hdac7 macrophages (Figures 1C and S1B). Conversely, Cre-mediated *Hdac7* deletion from macrophages (Figure S1C) selectively reduced Il-12p40 release in response to sub-maximal LPS doses (Figure 1D, top; Figures S1D and S1E), whereas NO production and inducible tumor necrosis factor (TNF) were unaffected (Figure 1D, bottom; Figures S1F–S1H). However, at a maximal stimulatory concentration of LPS (10 ng/mL), inducible Il-12p40 production was not reduced in *Hdac7*-deficient macrophages (Figure S1E). This likely reflects redundancy with other class IIa HDACs at high LPS concentrations (see ahead).

Hdac7 Interacts with the Proinflammatory and Glycolytic Enzyme Pkm2

To gain mechanistic insights, we next used the V5 epitope tag on the ectopically expressed Hdac7 in Mac-Hdac7 mice (Figure 1A), performing rapid immunoprecipitation mass spectrometry of endogenous proteins (RIME) (Mohammed et al., 2016) to identify Hdac7-interacting proteins in macrophages. Unexpectedly, two of the top eight proteins identified, which were not identified in macrophages from either of the littermate control lines, were glycolytic enzymes (Pkm and Gapdh; Figure 2A). Gapdh (Kornberg et al., 2018) and Pkm2 (Yang et al., 2014; Palsson-McDermott et al., 2015; Shirai et al., 2016) have both been linked to control of immunometabolism and inflammation. In this study we focused on the role of the latter in functional interplay with Hdac7. Proximity ligation assays (PLAs) using Mac-Hdac7 macrophages confirmed a specific interaction between Hdac7-V5 and Pkm2 in macrophages (Figure 2B). A PLA signal was not detected when using either MacBlue macrophages with the same antibody pair or an isotype control antibody against a cytoplasmic enzyme (p38) in Mac-Hdac7 macrophages. The specificity of the interaction was independently confirmed, as Pkm2 co-immunoprecipitated with Hdac7-V5, but not Hdac6-V5 (a class IIb HDAC) or another unrelated V5-tagged protein (Sox7-V5), in HEK293T cells (Figure 2C).

In addition to their C-terminal deacetylase domain, class IIa HDACs also harbor an N-terminal protein-binding domain that provides non-enzymatic functions (Chatterjee et al., 2011; Ma and D'Mello, 2011). We therefore determined if Hdac7 enzymatic activity was of relevance to the interaction with Pkm2. First, we used a *Leishmania tarentolae* cell-free protein expression system (Kovtun et al., 2011) to generate recombinant Pkm2, as well as

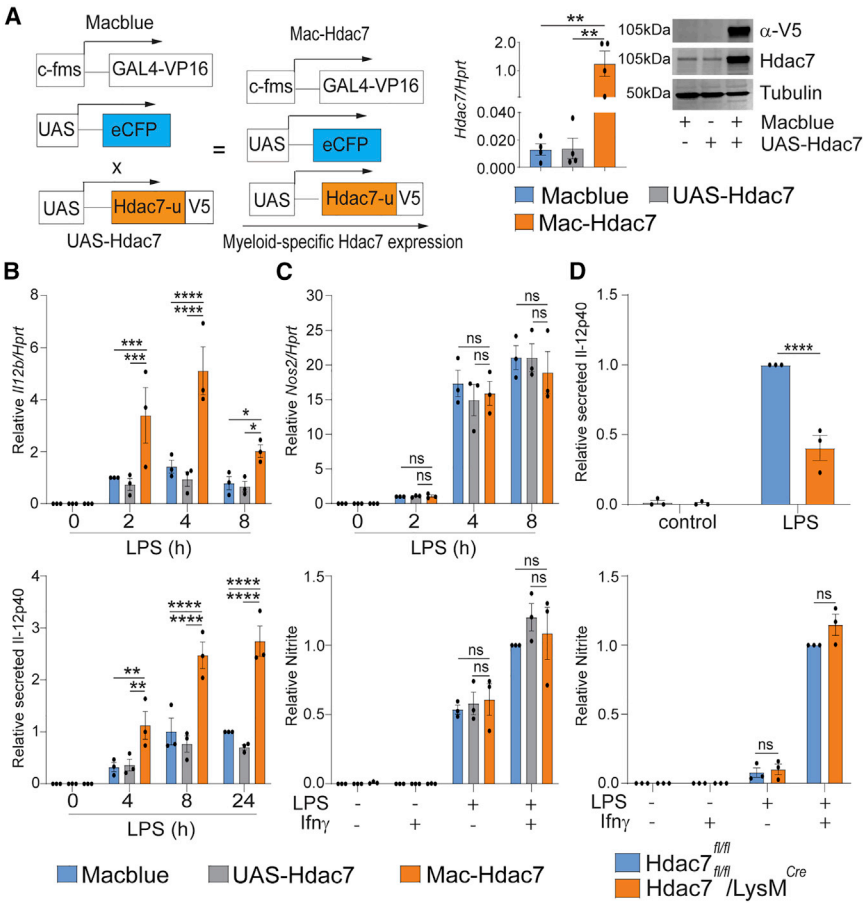

Figure 1. Hdac7 Drives Selective Inflammatory Responses in Macrophages

(A) Offspring of MacBlue x UAS-Hdac7 crosses inheriting both transgenes (Mac-Hdac7 mice) express Hdac7 in myeloid cells (left). *Hdac7* mRNA (middle) and Hdac7 protein (right) in BMMs from Mac-Hdac7 mice versus littermate control mice. Data (mean + SEM, n = 4) are combined from four experiments (middle) or are representative of four experiments (right) (**p < 0.01).

(B) Indicated BMM populations were treated with LPS (100 ng/mL), and *Il12b* mRNA (top) and secreted Il-12p40 (bottom) were quantified (qPCR, ELISA).

(C) Indicated BMM populations were treated with LPS (100 ng/mL), and *Nos2* mRNA was quantified using qPCR (top). BMMs were primed with Ifnγ (5 ng/mL) for 18 h, then treated with LPS (100 ng/mL) for 24 h, after which NO production was assessed (bottom).

(D) BMMs from *Hdac7*$^{fl/fl}$/*LysM*^{Cre} and littermate control mice were stimulated with LPS (0.5 ng/mL) for 4 h. Secreted Il-12p40 was determined (top). Additionally, BMMs were primed with Ifnγ (5 ng/mL) for 18 h, then treated with LPS (0.5 ng/mL) for 24 h, after which NO production was assessed (bottom).

Graphical data (mean ± SEM, n = 3) were normalized to the MacBlue control for (B) and (C) or to the *Hdac7*$^{fl/fl}$ control for (D) and are combined from three experiments. Statistical significance for (B)–(D) was determined using two-way ANOVA, followed by Tukey's multiple-comparison test (ns, not significant; **p < 0.01, ***p < 0.001, and ****p < 0.0001).

See also Figure S1.

the C-terminal (deacetylase-containing) and N-terminal (protein-binding) domains of Hdac7 (Figure 2D, top). Using AlphaLISA assays, we found that Pkm2 directly and selectively interacts with the C-terminal deacetylase-containing domain of Hdac7 (Figure 2D, bottom). We next created a putative enzyme-dead variant of Hdac7 (Hdac7ΔH649A) by mutating a conserved histidine (H649) (Figure 2E) that is present in the Hdac7 catalytic pocket (Figure 2F; conserved residue is H672 in human HDAC7). The corresponding residue was required for HDAC4 enzymatic activity (Fischle et al., 2002). We confirmed that this mutation ablated enzymatic activity in a cell-based class IIa deacetylase activity assay (Figure 2G, left), without affecting protein expression (Figure 2G, right). Enzyme-substrate interactions are generally unstable and transient, and point mutations that inactivate enzymatic activity of a protein often stabilize its interaction with substrate(s). We found that the interaction between Hdac7 and Pkm2 was enhanced when using the enzyme-dead mutant (Figure 2H), thus suggesting that Hdac7 may post-translationally modify Pkm2 or a component(s) of the complex.

The Inflammatory Effects of Hdac7 Are Mediated by Immunometabolism

Given that Hdac7 interacted with Pkm2, we postulated that the proinflammatory functions of Hdac7 might be linked to immunometabolic control. Indeed, Mac-Hdac7 macrophages displayed increased LPS-inducible lactate, elevated production of the glycolysis-linked proinflammatory mediators Il-1β (Palsson-McDermott et al., 2015) and Ccl2 (Lee et al., 2018) and reduced Il-10 production (Mills et al., 2016; Figures 3A–3D). These effects were mirrored at the mRNA level (Figures S2A–S2C). To determine if there is a causal link between the effects of Hdac7 on LPS-inducible glycolysis and the immunometabolism-associated cytokine profile in macrophages, we inhibited glucose uptake with 2-deoxy-D-glucose (2-DG). As anticipated, 2-DG abrogated the increased production of Il-1β and Ccl2 that was apparent in Mac-Hdac7 versus littermate control macrophages (Figures S2D and S2E). In contrast, although secreted Tnf was also amplified in LPS-activated Mac-Hdac7 BMMs, 2-DG treatment did not affect this response (Figure S2F). This is consistent with not all macrophage inflammatory responses being directly controlled by TLR-inducible glycolysis.

To further characterize the involvement of Hdac7 in LPS-induced metabolic control, macrophages from *Hdac7*$^{fl/fl}$/*LysM*^{Cre} mice (*Hdac7*-deficient BMMs) were subjected to metabolic flux analysis (Figure S2G). Although there was no apparent difference in an unstimulated state (Figure 3E), the extracellular acidification rate (ECAR) was significantly reduced in LPS-stimulated *Hdac7*-deficient macrophages (Figure 3F). This translated

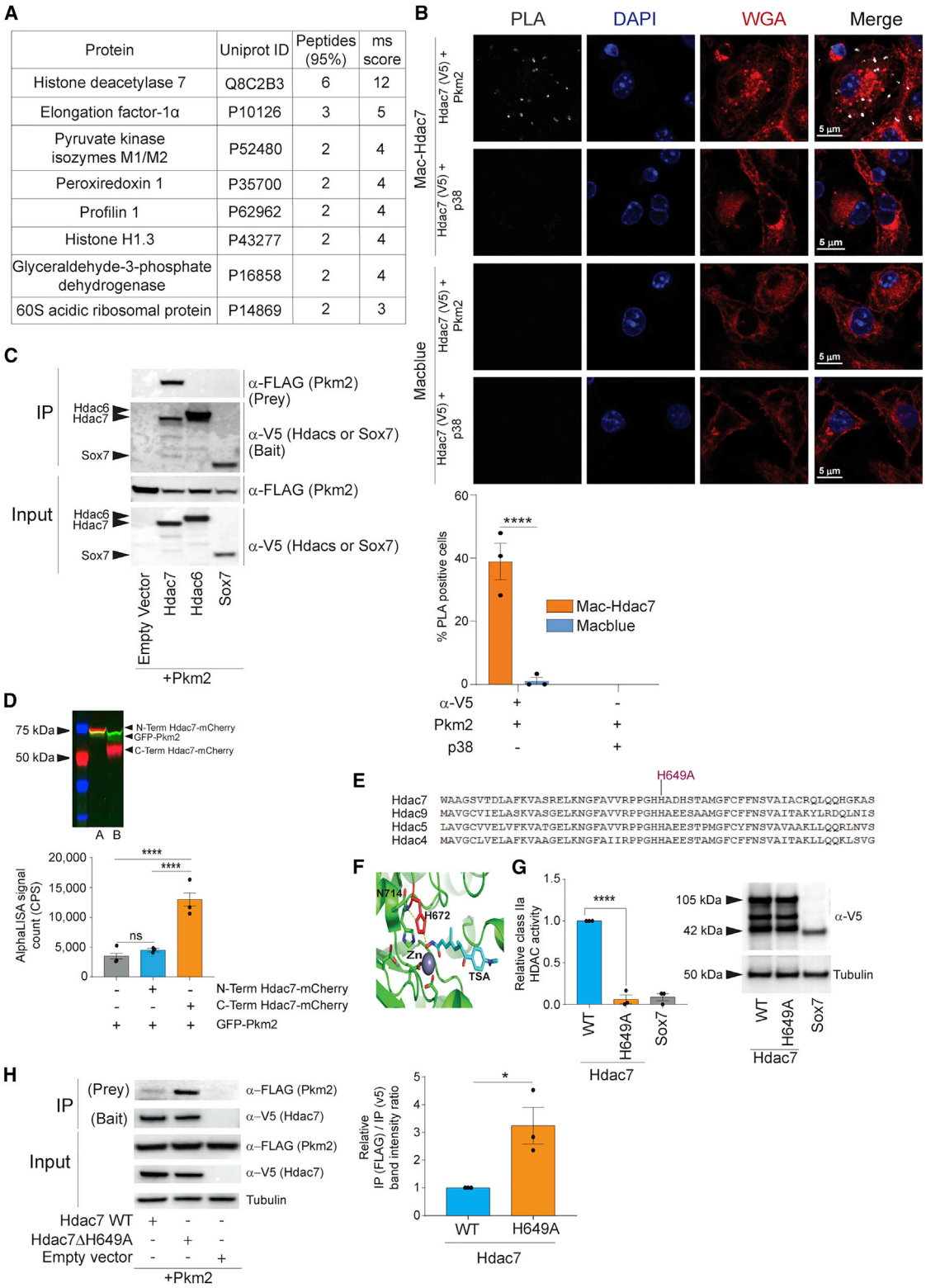

Figure 2. Proinflammatory Hdac7 Interacts with the Glycolytic Enzyme Pkm2

(A) The top 8 Hdac7-interacting proteins in macrophages, as identified using RIME.

(B) PLA was performed on Mac-Hdac7 BMMs, using antibodies against endogenous Pkm2 and the V5 epitope tag of Hdac7 (left column). The α-V5 antibody and an antibody recognizing MAPK p38 (of the same isotype as the α-PKM2 antibody) were used as a specificity control. PLA was also performed in parallel on

(legend continued on next page)

to a significant reduction in LPS-induced glycolysis, maximum glycolytic capacity, and secreted lactate, while the overall glycolytic reserve was unaffected (Figures 3G–3J). LPS-inducible glucose uptake, as assessed using 2-NBDG fluorescence, was also significantly reduced (Figure 3K). This altered metabolic phenotype observed in *Hdac7*-deficient macrophages was largely restricted to glycolysis, as the differences in mitochondrial respiration in control and LPS-activated *Hdac7*-deficient versus control macrophages, as measured by oxygen consumption rate (OCR), were much less pronounced (Figure S2H). Consistent with the attenuated glycolytic response in *Hdac7*-deficient macrophages, LPS-nigericin-triggered Il-1β (Figure 3L) and LPS-induced Ccl2 (Figure 3M) were also reduced. These effects were again selective for sub-maximal doses of LPS, with no differences observed in secreted Il-1β and Ccl2 production from *Hdac7*-deficient macrophages at a maximal stimulatory LPS concentration (10 ng/mL) (Figures S2I and S2J). We next assessed these responses in human macrophages. Differentiation of human macrophages from their monocytic precursors resulted in markedly increased HDAC7 expression (Figure S3A), and *HDAC7* silencing in these cells (Figure S3B) reduced both nigericin-triggered IL-1β release from LPS-primed cells (Figure S3C) and LPS-induced CCL2 (Figure S3D). In contrast, TNF was unaffected (Figure S3E). Thus, HDAC7 also promotes the production of immunometabolism-linked inflammatory mediators in human macrophages.

The Proinflammatory Functions of Hdac7 and Pkm2 Are Interdependent

The transcription factor Hif1α has been implicated in the proinflammatory effects of both Pkm2 (Palsson-McDermott et al., 2015; Shirai et al., 2016) and Hdac7 (Shakespear et al., 2013) in macrophages. Hif1α also acts as a link between regulated metabolism and Il-1β production in macrophages (Tannahill et al., 2013). We therefore next assessed the functional interplay among Hdac7, Pkm2, and Hif1α in macrophage inflammatory responses. Retroviral Pkm2 overexpression amplified nigericin-triggered Il-1β release from LPS-primed BMMs (Figures 4A and S4A) without affecting LPS-induced Tnf (Figures 4B and S4B). However, Pkm2 had no such effect in *Hdac7*-deficient macrophages (Figures 4A and S4A). The amplifying effect of Pkm2 on Il-1β release was also blocked by small-molecule inhibitors of Hif1α (Shirai et al., 2016; Figures 4A and S4A) or class IIa HDACs (Lobera et al., 2013) (TMP269; Figures S4C, S4D, and 4C), with these compounds having no effect on Tnf (Figures 4B, 4D, S4B, and S4E). Collectively, these data suggest that the capacity of Pkm2 to selectively drive macrophage inflammatory responses requires both Hdac7 and Hif1α. Conversely, antagonizing the proinflammatory functions of Pkm2 with either DASA (Palsson-McDermott et al., 2015; Figures 4E and S4F) or a HIF1α inhibitor (Figures 4F and S4G) blocked Il-1β amplification in Mac-Hdac7 macrophages. These effects were selective, with Tnf production being unaffected by either compound (Figures S4H and S4I). Thus, the immunometabolism-linked proinflammatory effects of Hdac7 require both Pkm2 and Hif1α. Interestingly, LPS-induced Tnf was elevated in Mac-Hdac7 macrophages (Figures S4H and S4I), suggesting an additional role for this HDAC beyond glycolysis-dependent inflammatory responses.

To further evaluate mechanisms by which Hdac7 may act, we next assessed whether Hdac7 inhibition by TMP269 (Figure S4C) affects the formation of Pkm2 monomers and dimers, as these have been linked to its proinflammatory effects (Palsson-McDermott et al., 2015). We first confirmed that TMP269 had no effect on total Pkm2 protein levels (Figure 4G). Size exclusion chromatography revealed that Pkm2 exists as a mix of high- and low-molecular weight complexes in unstimulated BMMs (Figure 4H). LPS treatment skewed this towards low-molecular weight forms of Pkm2, consistent with its transition from a glycolytic tetramer to the proinflammatory dimers and/or monomers. TMP269 interfered with this LPS-induced transition, with a similar effect being observed with DASA (Figure 4H) that induces PKM2 tetramer formation (Anastasiou et al., 2012) and inhibits PKM2 proinflammatory functions (Palsson-McDermott et al., 2015). The phosphorylation of Pkm2 on Y105 is thought to promote formation of a dimeric form of Pkm2 that has reduced pyruvate kinase (PK) activity and localizes to the nucleus (Prakasam et al., 2018). We therefore next examined if Hdac7 activity was required for Pkm2 phosphorylation on Y105 and/or its nuclear localization. Surprisingly, Hdac7 and phospho-Y105 Pkm2 both localized to the cytoplasm in BMM activated with LPS for 4 h (Figure 4I). Moreover, the cytoplasmic phospho-Y105 Pkm2 dimer was also detectable under denaturing conditions, with TMP269 treatment reducing its levels. Class IIa HDAC inhibition had no obvious effect on monomeric phospho-Y105 Pkm2 in the cytoplasm, and neither Pkm2 monomers nor dimers

MacBlue BMMs that do not express Hdac7-V5. Images (top) are representative of three independent experiments (DAPI, DNA; WGA, cell membranes). The percentages of PLA-positive cells in each experiment were also quantified (bottom). (Scale bar, 5 μM).

(C) HEK293T cells were transfected with Pkm2-FLAG and the indicated V5-tagged constructs. Co-immunoprecipitations were performed using V5-tagged proteins as bait (α-V5 IP) and cell lysates were analyzed using immunoblotting (anti-FLAG). Similar results were obtained in four experiments.

(D) SDS-PAGE analysis of *in vitro* co-translated Hdac7 domains and Pkm2 protein pair (A, N-term Hdac7-mCherry/GFP-Pkm2; B, C-term Hdac7-mCherry/GFP-Pkm2) (top). AlphaLISA analysis of Hdac7:Pkm2 interaction (bottom).

(E) Multiple sequence alignment of murine class IIa Hdacs, highlighting histidine 649 in Hdac7.

(F) A model of the active site of human HDAC7 in complex with TSA.

(G) HEK293T cells were transfected with the indicated constructs. After 24 h, class IIa HDAC enzyme assays were performed on cell lysates (left). Data were normalized to the WT Hdac7-V5 control. Lysates were also probed for the V5 tag to confirm expression (right).

(H) HEK293T cells were co-transfected the indicated constructs, and co-immunoprecipitated Pkm2-FLAG was detected using immunoblotting. Intensity of Pkm2-FLAG relative to the V5-tagged bait was quantified using densitometry (ImageLab), then normalized to the WT Hdac7-V5 control.

Graphical data (mean ± SEM, n = 3) are combined from three experiments. Statistical significance was determined using one-way ANOVA for (D) and (G) and two-way ANOVA for (B), followed by Tukey's (D and G) and Sidak's (B) multiple-comparison tests or an unpaired t test for (H) (ns, not significant; *$p < 0.05$ and ****$p < 0.0001$).

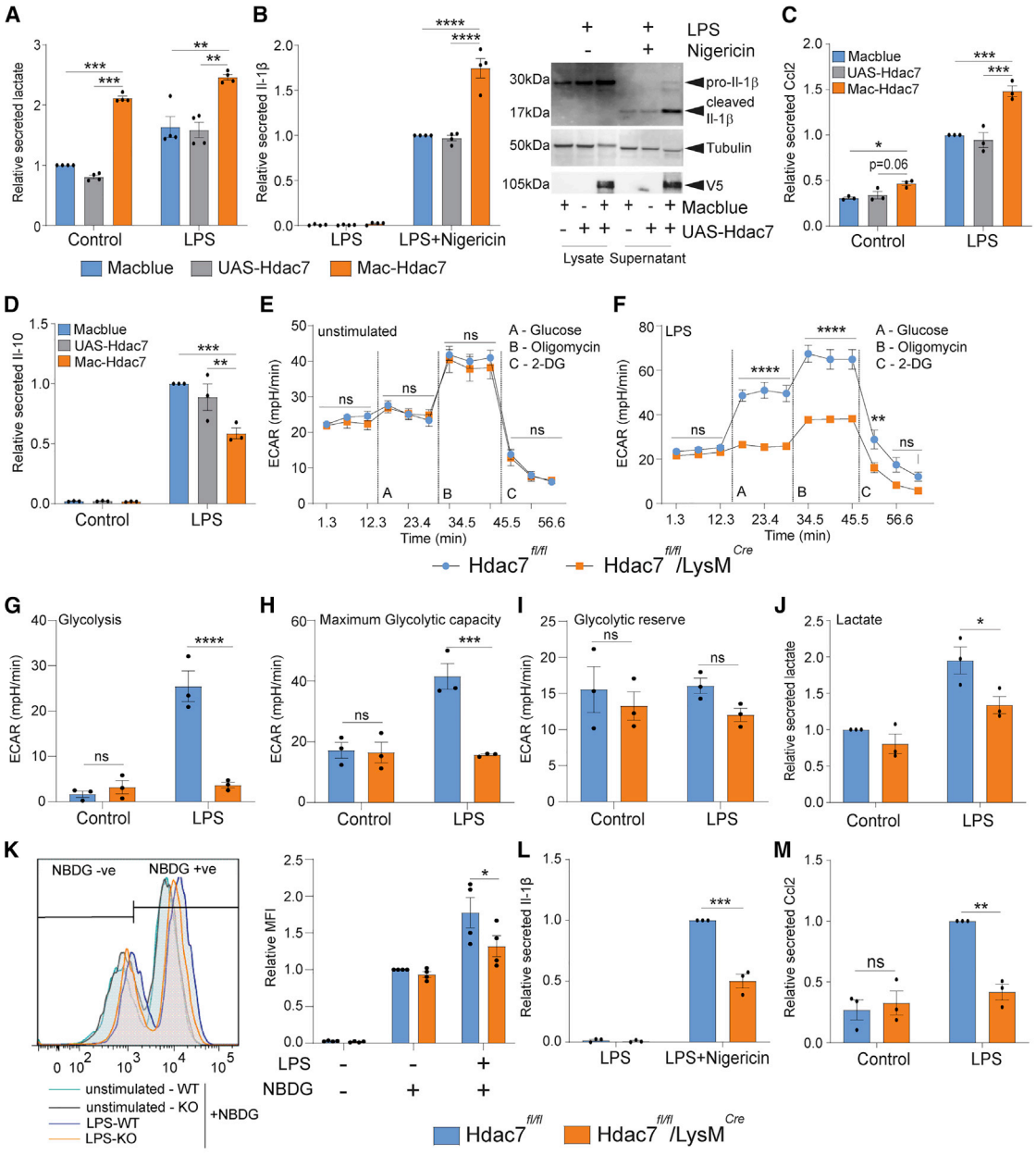

Figure 3. Hdac7 Promotes Macrophage Glycolytic and Inflammatory Responses

(A) The indicated BMM populations were treated with or without LPS (100 ng/mL) for 24 h, and extracellular lactate concentrations were determined.

(B–D) BMM were treated with LPS (100 ng/mL, 4 h), and levels of nigericin-triggered Il-1β release (B, left) were quantified. Immunoblotting was performed on cell lysates and culture supernatants for cleaved and pro-Il-1β (B, right; representative of three experiments). Supernatants from LPS-treated BMMs were also analyzed for secreted Ccl2 (C) and Il-10 (D).

(E–J) The indicated BMM populations were either left untreated (E) or treated with LPS (0.5 ng/mL, 24 h) (F). ECAR was then measured using a Seahorse XFe96 analyzer, and cell counting by Hoechst was used to normalize the data for any differences in plating density. Glycolytic parameters were calculated from measured ECAR levels (G–I). Secreted extracellular lactate was also determined (J).

(K) The indicated BMM populations were treated with LPS (0.5 ng/mL, 24 h), and glucose uptake was assessed using NBDG fluorescence. A representative flow cytometry plot (left), as well as mean fluorescence intensity (MFI) data (right), are shown.

(L and M) The indicated BMM populations were treated with LPS (0.5 ng/mL, 4 h), and levels of nigericin-triggered Il-1β release (L) and Ccl2 (M) were determined. Graphical data were normalized to the MacBlue control for (A)–(D) and the *Hdac7*$^{fl/fl}$ control for (J), (L), and (M). Graphical data in (A)–(M) (mean ± SEM) are combined from at least three independent experiments. Statistical significance for (A)–(M) was determined using two-way ANOVA, followed by Tukey's (A–D) and Sidak's (E–M) multiple-comparison test (*p < 0.05, **p < 0.01, ***p < 0.001, and ****p < 0.0001). See also Figures S2 and S3.

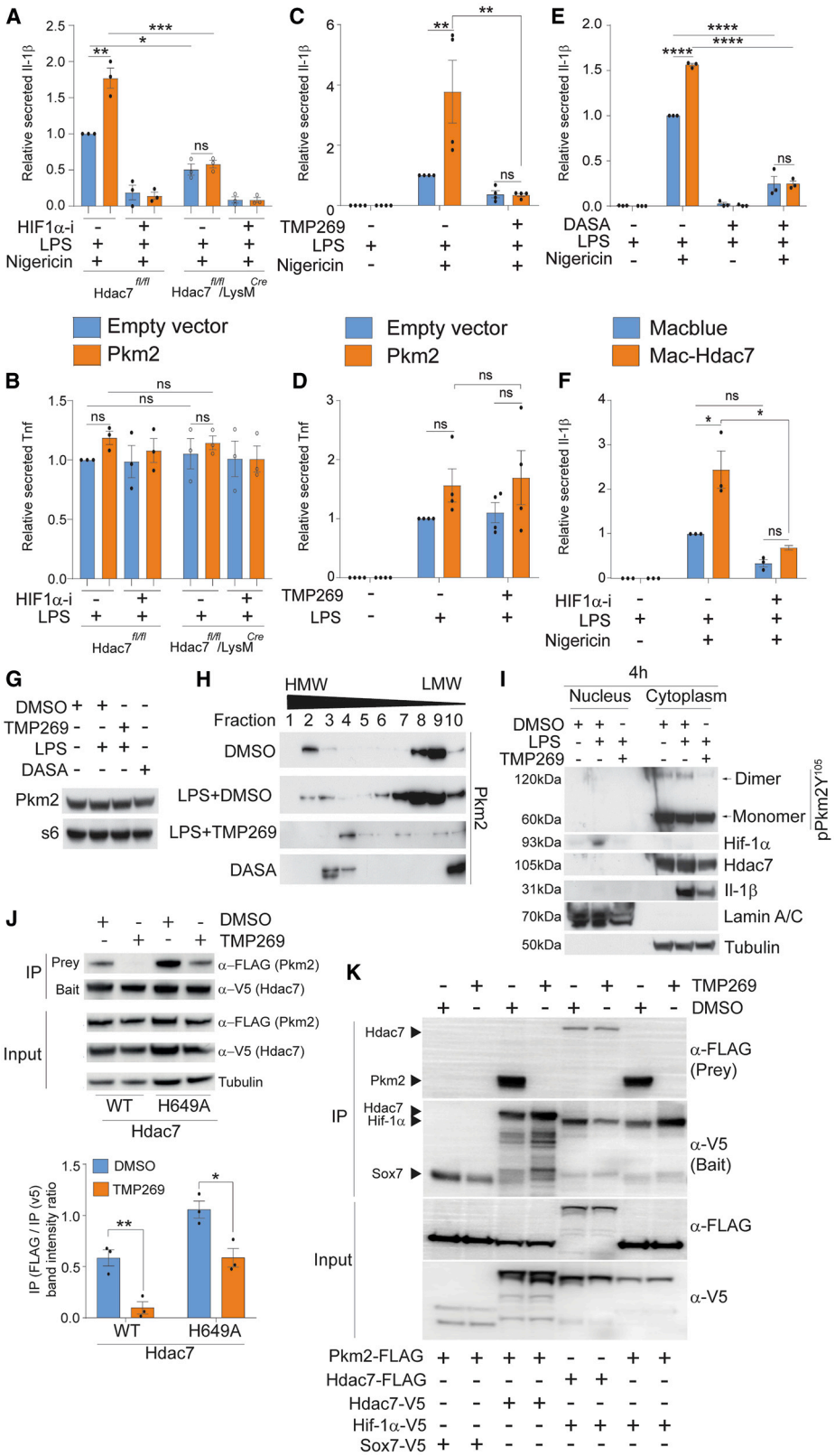

(legend on next page)

could be detected in the nucleus under our experimental conditions. In contrast, LPS-inducible Hif1α was readily detectable in the nucleus, with TMP269 abolishing this response.

Because Pkm2 interacts with the deacetylase-containing domain of Hdac7 (Figure 2D), we considered that TMP269 may disrupt the interaction between Hdac7 and Pkm2. To examine this possibility, we assessed the effect of TMP269 on formation of the Hdac7-Pkm2 complex. Indeed, TMP269 reduced the interaction between Pkm2 and both wild-type and the enzyme-dead mutant of Hdac7 (ΔH649A) (Figure 4J), suggesting that this compound prevents Pkm2, or a component of the complex, docking into the Hdac7 catalytic site. TMP269 also disrupted the Pkm2-Hif1α interaction but not the Hdac7-Hif1α interaction (Figure 4K). This suggests that the direct interaction between Hdac7 and Pkm2 (Figure 2D) is likely required for the assembly of a Pkm2/Hdac7/Hif1α complex that permits nuclear translocation of Hif1α to drive immunometabolism-associated inflammatory responses. Collectively, these data suggest that the Hdac7-Pkm2 complex acts in the cytoplasm to skew immunometabolism-associated inflammatory responses in macrophages, likely by enabling nuclear Hif1α localization.

Deacetylation of Pkm2 Permits LPS-Inducible Glycolysis and Associated Inflammatory Responses

Next, we examined the requirement for Hdac7 enzymatic activity in proinflammatory responses by retrovirally overexpressing Hdac7 and its enzyme-dead mutant in *Hdac7*-deficient macrophages. Only enzymatically active Hdac7 amplified nigericin-triggered Il-1β release in macrophages primed with a submaximal LPS dose (Figures 5A and S5A), and Hdac7 did not affect LPS-induced Tnf in this system (Figures 5B and S5B). We then assessed if PK activity was influenced by Hdac7. In HEK293T cells transfected with Pkm2, co-transfection with wild-type but not enzyme-dead Hdac7 enhanced PK activity (Figure 5C). Furthermore, PK activity was increased in LPS-activated macrophages, and this response was attenuated by treatment with TMP269 (Figure S5C) or by *Hdac7* deletion (Figure 5D).

We next assessed potential Hdac7-mediated post-translational modifications of Pkm2. Immunoprecipitation experiments in HEK293T cells confirmed that TMP269 treatment increased Pkm2 acetylation (Figure 5E). To identify candidate lysine residues targeted by class IIa HDACs, immunoprecipitated Pkm2 was subjected to mass spectrometry. The lysine residue at position 89 (K89) was the most promising candidate, as it was acetylated in cells treated with a class IIa HDACi but not in controls cells (Figure S5D). However, previous studies on Pkm2 in other cell systems have identified roles for K305 in regulating stability (Lv et al., 2011) and K433 in controlling localization (Lv et al., 2013). Although our approach was not quantitative, we did detect acetylation at both K305 and K433 (Figures S5E and S5F) and found that this was increased upon TMP269 treatment (K305, 1.46-fold; K433, 1.52-fold; average of two experiments).

To assess roles for these lysine residues in Pkm2-driven inflammatory responses, we generated K-to-R acetyl-dead mimics (K89R, K305R, K433R) of Pkm2 and confirmed their expression in HEK293T cells (Figure 5F). Our prediction was that one or more of these would be hyperactive in driving inflammatory responses, as they would act as constitutively deacetylated forms of Pkm2. Whereas the K89R and K305R mutants of Pkm2 were similarly active to wild-type Pkm2 in amplifying nigericin-triggered Il-1β release from LPS-primed macrophages, the K433R mutant was hyperactive (Figure 5G). Furthermore, the recently characterized class IIa HDACi, TMP195 (Guerriero et al., 2017), attenuated this response for wild-type, K89R, and K305R Pkm2, whereas the K433R mutant was resistant to this effect. These data are in keeping with a model in which Hdac7 deacetylates Pkm2 at K433 to license its inflammatory functions. Indeed, when overexpressed in *Hdac7*-deficient macrophages, wild-type Pkm2, as well as the K89R and K305R mutants, did not enhance Il-1β production in response to low-dose LPS. In contrast, the K433R mutant retained its activity (Figure 5H). Both wild-type and the K433R mutant of Pkm2 localized to the cytoplasm of macrophages (Figure 5I), consistent with our analysis of endogenous Pkm2 localization by sub-cellular fractionation (Figure 4I). Collectively, these data suggest a role for Hdac7 in deacetylating cytoplasmic Pkm2 for initiation of proinflammatory responses.

Figure 4. Hdac7-Pkm2-Hif1α Interactions and Associated Inflammatory Responses

(A and B) The indicated BMM populations were retrovirally transduced with empty vector or Pkm2 constructs and treated with 0.5 ng/mL LPS for 4 h with or without a HIF1α inhibitor (HIF1αi, 10 μM), and levels of nigericin-triggered Il-1β (A) and Tnf (B) were measured.

(C and D) BMM were retrovirally transduced as above, then treated with 100 ng/mL LPS for 4 h with or without TMP269 (30 μM). Levels of nigericin-triggered Il-1β (C) and Tnf (D) were measured.

(E and F) The indicated BMM populations were treated with LPS (100 ng/mL) with or without DASA (10 μM) for 4 h (E) or a HIF1αi (10 μM) (F) for 8 h, after which levels of nigericin-triggered Il-1β were measured.

(G and H) BMM were treated with DMSO, TMP269 (30 μM), LPS (100 ng/mL), and/or DASA (50 μM) for 24 h, as indicated. Pkm2 protein in whole cell lysates (G) or following fractionation by size exclusion (H) was detected using immunoblotting. Data are representative of two experiments.

(I) BMMs were stimulated with LPS (100 ng/mL) for 4 h with or without TMP269 (30 μM). Nuclear and cytoplasmic fractions were separated and the indicated proteins were detected using immunoblotting. The displayed immunoblot is representative of three experiments.

(J) HEK293T cells were transfected with indicated constructs. At 8 h post-transfection, cells were treated with either DMSO or TMP269 (30 μM), and cell lysates were collected at 24 h post-transfection. Co-immunoprecipitations were performed using V5-tagged proteins as bait (anti-V5 IP), and cell lysates were analyzed using immunoblotting (anti-FLAG) (top, representative of three experiments). Densitometric quantification of band intensities (bottom, ImageLab).

(K) HEK293T cells were transfected with the indicated constructs. At 8 h post-transfection, cells were treated with either DMSO or TMP269 (30 μM), and cell lysates were collected at 24 h post-transfection. Immunoprecipitated proteins (with V5-tagged proteins as bait) were detected using immunoblotting. The displayed immunoblot is representative of three experiments.

Graphical data (mean + SEM, n = 3 or 4) are combined from three or four experiments. Statistical significance was determined using two-way ANOVA (A–F and J), followed by Tukey's multiple-comparison test (ns, not significant; *p < 0.05, **p < 0.01, ***p < 0.001, and ****p < 0.0001). See also Figure S4.

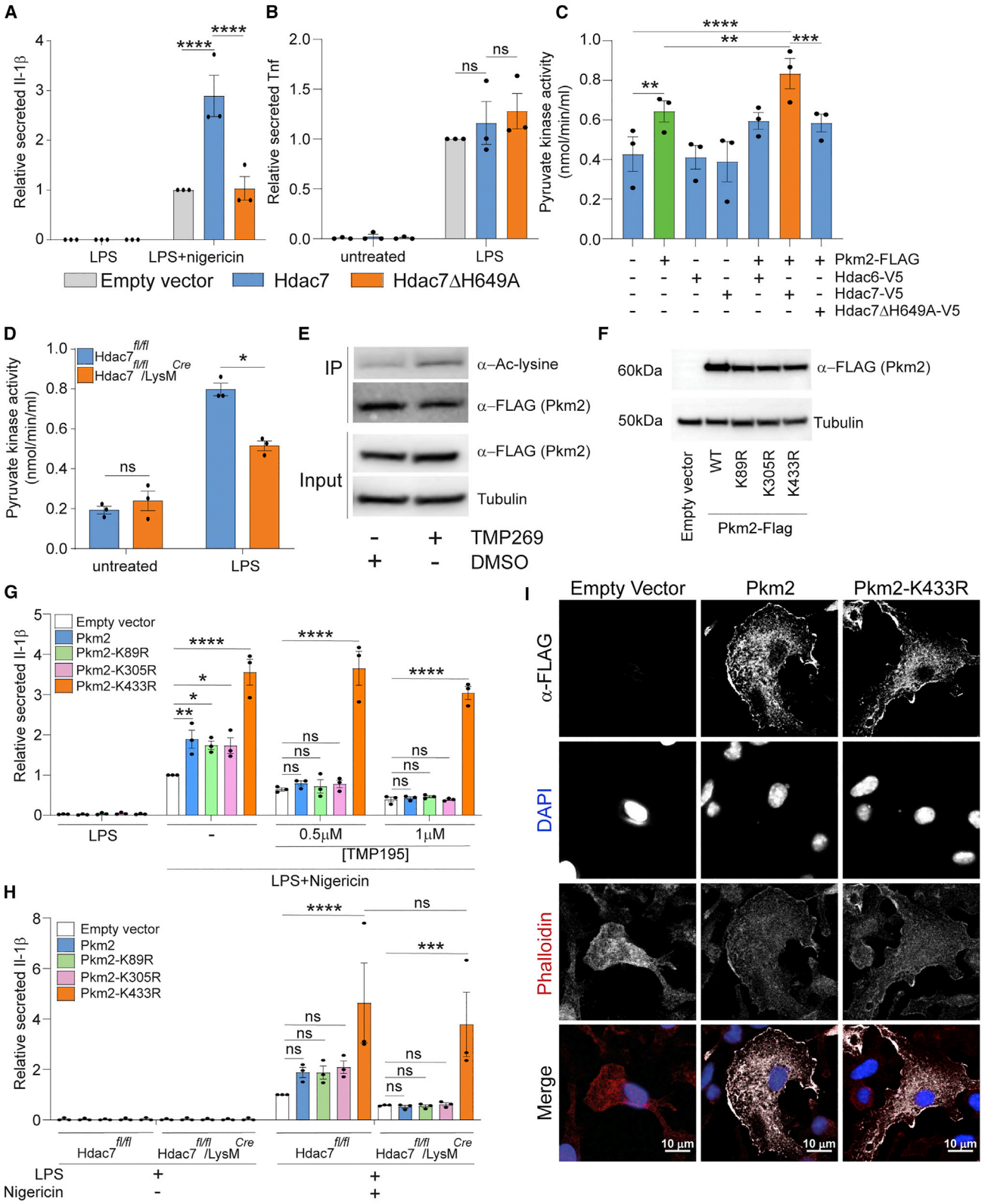

(legend on next page)

Targeting of Class IIa HDACs Inhibits TLR-Inducible Glycolysis and Associated Inflammatory Responses in Macrophages

Given the redundant nature of Hdac7 in macrophages responding to maximal stimulatory LPS concentrations (Figures S1E, S2I, and S2J) and the high level of conservation in class IIa HDAC deacetylase domains (Hsu et al., 2017), we considered that multiple class IIa HDACs may act through the Pkm2 immunometabolic axis described here. We previously showed that the Hdac7-u isoform of Hdac7 has a selective role in promoting inflammatory responses in RAW 264.7 macrophages, likely due to its inability to interact with the transcriptional repressor Ctbp (Shakespear et al., 2013). We found that the *Ctbp/Hdac7* ratio is much higher in RAW 264.7 cells than in BMMs (Figure 6A), consistent with a selective role for Hdac7-u in driving inflammatory responses in the former cell population. Thus, we questioned whether other class IIa HDACs might also act upstream of Pkm2.

Co-immunoprecipitation studies in HEK293T cells showed that other class IIa HDACs interact with Pkm2 (Figure 6B). We thus predicted that pharmacological targeting of the class IIa HDAC family would attenuate inducible glycolysis and associated inflammatory responses in macrophages responding to maximal stimulatory LPS concentrations. Indeed, in BMMs treated with 100 ng/mL LPS, TMP269 markedly reduced levels of several glycolytic intermediates (Figure S6A; Table S1), also attenuating extracellular media acidification (Figure S6B) and lactate production (Figure S6C). In contrast, the HDAC6 inhibitor tubastatin A had no effect on LPS-induced lactate (Figure S6D). LPS-inducible *Il1b* mRNA (Figure S6E) and nigericin-triggered Il-1β release in LPS-primed BMMs (Figure S6F) were also dramatically reduced. However, TMP269 did not affect nigericin-triggered cell death (Figure S6G), consistent with a requirement for class IIa HDAC enzymatic activity in *Il1b* transcriptional control, rather than inflammasome activation. TMP269 also inhibited LPS-inducible secretion of Ccl2 (Figure S6H) and increased Il-10 levels (Figure S6I), consistent with our earlier findings using Mac-Hdac7 macrophages (Figures 3C and 3D). Interestingly, TMP269 did not affect secreted Tnf (Figure S6J). Given that LPS-induced Tnf production was amplified in Mac-Hdac7 BMM (Figures S2F, S4H, and S4I), Hdac7 may exert additional effects independently of its enzymatic function. Collectively, our data suggest that class IIa HDAC enzyme activity is required for LPS-inducible glycolysis and associated inflammatory outputs, likely via the Pkm2 axis.

We next silenced the class IIa *Hdac* family in primary macrophages. Small interfering RNA (siRNA)-mediated knockdown of *Hdac7* reduced nigericin-triggered Il-1β in BMM primed with a maximal stimulatory LPS concentration (Figures 6C and S6K). Inhibiting residual class IIa HDAC activity with TMP195 reduced levels of secreted Il-1β in control and *Hdac7*-silenced BMM (Figure 6C). Importantly, silencing of all class IIa HDACs resulted in a further reduction in secreted Il-1β, and TMP195 had no additional inhibitory effect (Figure 6C). In contrast, LPS-induced Tnf production was unaffected (Figure 6D). A similar phenotype was observed upon genetically knocking down class IIa HDACs in PMA-differentiated THP-1 (Figures S6L and S6M). These data indicate that multiple class IIa HDACs can promote LPS-inducible IL-1β production in human and mouse macrophages and also confirm that the inhibitory effect of TMP195 on this response occurs via class IIa HDAC enzyme inhibition. Given this confirmation of TMP195 target specificity, we next assessed its effects on LPS-regulated macrophage metabolism. Similar to our earlier observations with *Hdac7*-deficient macrophages, TMP195 significantly reduced ECAR in BMMs but did not affect OCR (Figures 6E and 6F). TMP195 also significantly reduced LPS-induced 2-NBDG uptake, consistent with inhibition of glucose uptake (Figure 6G). Thus, class IIa HDACs drive inducible glycolysis and associated inflammatory responses in macrophages.

Hdac7 Drives Acute Inflammatory Responses *In Vivo*

To determine if the Hdac7-Pkm2 pathway amplifies inflammatory responses *in vivo*, the phenotype of Mac-Hdac7 mice after LPS challenge was next assessed. Levels of several HDAC-dependent proinflammatory mediators (Il-1β, Ccl2, and Il-12p40) in sera from Mac-Hdac7 mice were significantly elevated compared with littermate controls (Figures 7A–7C). Tnf levels were also increased (Figure S7A), consistent with our *in vitro* findings (Figures S2F, S4H, and S4I). Unexpectedly, Il-10 was also increased (Figure 7D), which likely reflects a compensatory mechanism to counter the hyper-inflammatory phenotype of LPS-challenged Mac-Hdac7 mice. Il-27 levels were also significantly increased and there was a trend for

Figure 5. Hdac7 Enzymatic Activity and Pkm2 Deacetylation Are Required for Glycolysis-Associated Inflammatory Responses

(A and B) BMMs from *Hdac7*$^{fl/fl}$/*LysM*^{Cre} mice were retrovirally transduced with the indicated constructs, then treated with 0.5 ng/mL LPS for 4 h. Levels of nigericin-triggered Il-1β (A) and Tnf (B) were measured.

(C and D) PK assays were performed on lysates from HEK293T cells transfected with the indicated constructs or on indicated BMM populations treated ± LPS (0.5 ng/mL) for 4 h.

(E) Pkm2-FLAG-transfected HEK293T cells were treated at 24 h post-transfection with TMP269 (30 μM) for another 24 h, after which α-FLAG immunoprecipitation and immunoblotting were performed. The displayed immunoblot is representative of three experiments.

(F) HEK293T cells were transfected with the indicated expression constructs, after which immunoblotting was performed on cell lysates (representative of three experiments).

(G) BMMs were retrovirally transduced with the indicated constructs, then treated with 100 ng/mL LPS for 4 h in the presence or absence of TMP195 (0.5 or 1 μM). Levels of nigericin-triggered Il-1β were measured.

(H) BMMs from *Hdac7*$^{fl/fl}$ and *Hdac7*$^{fl/fl}$/*LysM*^{Cre} mice were retrovirally transduced with the indicated expression constructs, then treated with 0.5 ng/mL LPS for 4 h. Levels of nigericin-triggered Il-1β were measured.

(I) BMMs were retrovirally transduced with the indicated constructs and examined using immunofluorescence with an anti-FLAG antibody (DAPI, DNA; phalloidin, cell membranes). Images are representative of two independent experiments. (Scale bar, 10 μM).

Graphical data (mean + SEM, n = 3) are combined from three experiments. Statistical significance was determined using two-way ANOVA (A, B, D, G, and H) or one-way ANOVA (C), followed by Tukey's (A–C, G, and H) or Sidak's (D) multiple-comparison test (ns, not significant; *p < 0.05, **p < 0.01, ***p < 0.001, and ****p < 0.0001). See also Figure S5.

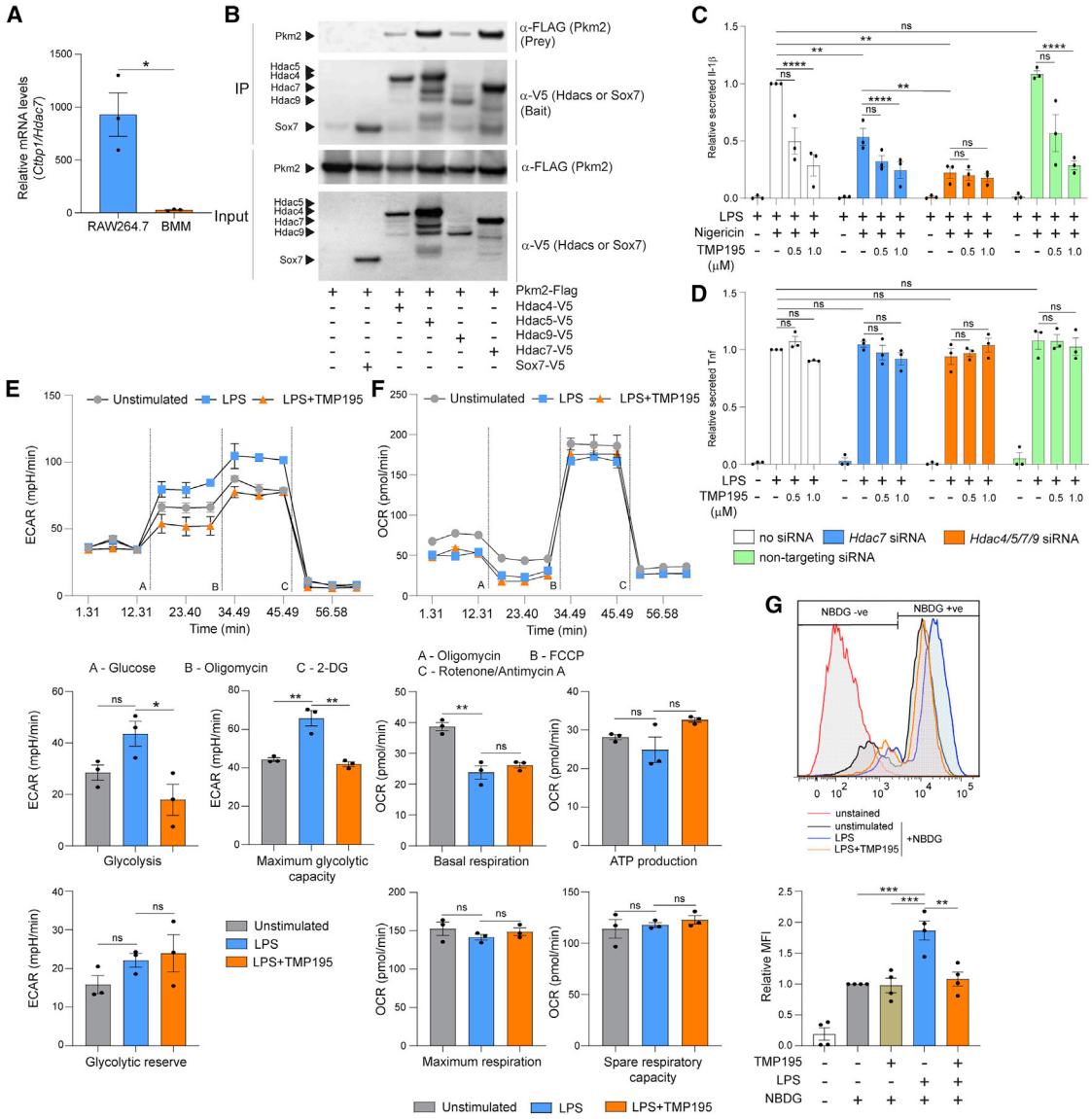

Figure 6. Targeting Class IIa HDACs Inhibits TLR-Inducible Glycolysis and Associated Inflammatory Responses in Macrophages

(A) mRNA levels of *Ctbp1* and *Hdac7* in unstimulated RAW 264.7 cells and BMMs were determined using qPCR, and a ratio of the two genes was plotted.

(B) HEK293T cells were co-transfected with the indicated constructs. Co-immunoprecipitations were performed using V5-tagged proteins as bait (anti-V5 IP), with Pkm2 interactions assessed using immunoblotting (anti-FLAG). The immunoblot is representative of three experiments.

(C and D) BMM were transfected with the indicated siRNAs and stimulated with LPS (100 ng/mL) for 4 h. Prior to LPS addition, transfected BMMs were pre-treated with or without TMP195 (0.5 or 1 μM) for 1 h. Levels of 1 h nigericin-triggered Il-1β release (C) and Tnf (D) in culture supernatants were measured.

(E and F) BMMs were pretreated with TMP195 (2 μM) for 1 h and then treated with or without LPS (100 ng/mL, 24 h). Metabolic flux analysis (ECAR [E, top] and OCR [F, top]) was performed using a Seahorse XFe96 analyzer, after which glycolytic (E, bottom) and mitochondrial (F, bottom) parameters were calculated.

(G) BMMs were pretreated with TMP195 (2 μM) for 1 h and then treated with or without LPS (100 ng/mL, 24 h). Glucose uptake was assessed using NBDG fluorescence.

Graphical data (mean + SEM, n = 3) are combined from three experiments. Statistical significance was determined using unpaired t test (A), two-way ANOVA (C and D), or one-way ANOVA (E–G), followed by Tukey's multiple-comparison test (ns, not significant; *p < 0.05, **p < 0.01, ***p < 0.001, and ****p < 0.0001). See also Figure S6 and Table S1.

increased Ifnγ (Figures S7B and S7C). To determine the effectiveness of class IIa HDAC inhibition in antagonizing the immunometabolism-associated inflammatory mediator shift after LPS challenge *in vivo*, we profiled TMP195 (Guerriero et al., 2017) in LPS-challenged C57BL/6J mice. This treatment abrogated hypothermia (Figure 7E) and significantly reduced serum levels of Il-1β and Il-12p40 (Figures 7F and 7G), with a trend toward enhanced circulating Il-10 levels (Figure 7H). Consistent with our *in vitro* observations (Figures 6D and S6J), the effects were again selective; Tnf levels were unaffected (Figure S7D). There

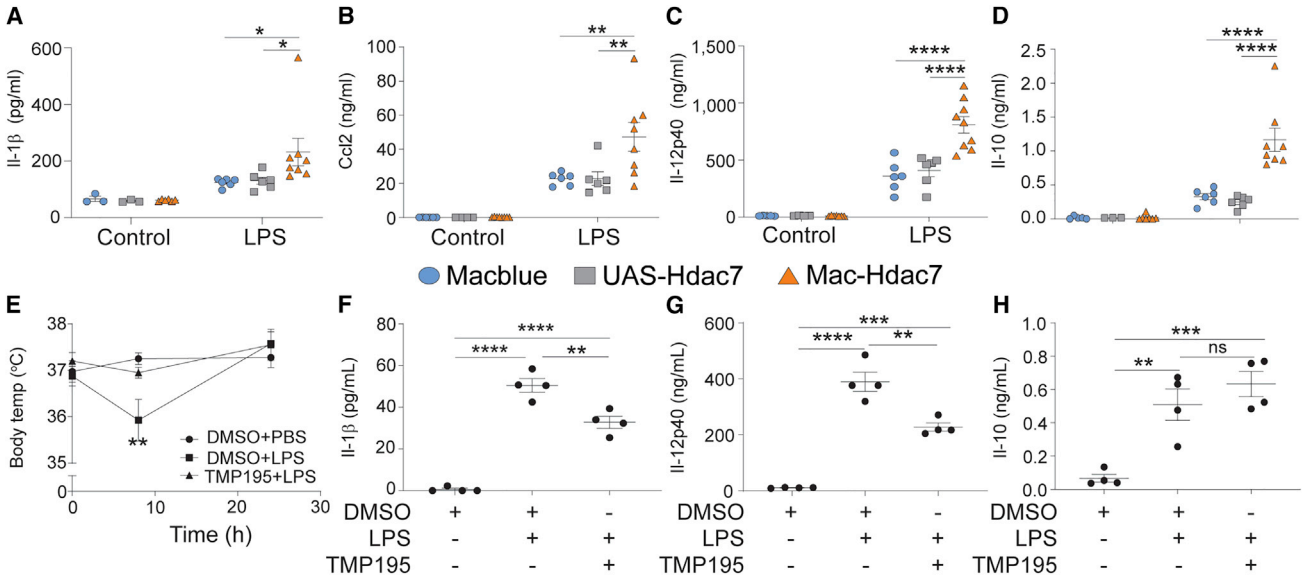

Figure 7. Hdac7 Drives Acute Inflammatory Responses *In Vivo*

(A–D) Mac-Hdac7 or littermate control mice were administered (intraperitoneal [i.p.]) LPS (2 mg/kg) or an equivalent volume of PBS. Sera were collected 4 h post-LPS challenge, and levels of Il-1β (A), Ccl2 (B), Il-12p40 (C), and Il-10 (D) were determined. Data are combined from two independent experiments (n = 10–15 mice per group in total).

(E–H) C57BL/6J mice were administered (i.p.) DMSO or TMP195 (50 mg/kg), as well as PBS or LPS (2 mg/kg), as indicated. (E) Core body temperature was measured at the indicated time points post-LPS challenge. Sera were collected at 4 h post-LPS challenge, and levels of Il-1β (F), Il-12p40 (G), and Il-10 (H) were determined. Data are mean + SEM of four mice per treatment group.

Statistical significance was determined using two-way ANOVA for (A)–(D) or one-way ANOVA for (E)–(H), followed by Tukey's multiple-comparison test (ns, not significant; *p < 0.05, **p < 0.01, ***p < 0.001, and ****p < 0.0001). See also Figure S7.

was also a trend for decreased Il-27 and Ifnγ (Figures S7E and S7F), consistent with our findings in LPS-challenged Mac-Hdac7 mice (Figures S7B and S7C). Thus, the glycolysis-associated class IIa HDAC-Pkm2 signaling axis can be pharmacologically targeted to suppress acute inflammation *in vivo*.

DISCUSSION

Otto Warburg's observation of enhanced aerobic glycolysis in rapidly proliferating cancer cells has been instructive for understanding how immune cells reprogram and coordinate metabolic and signaling pathways upon homeostatic disruption. The increase in aerobic glycolysis and the disruption in the TCA cycle upon macrophage activation enables the production of antimicrobial free radicals such as NO and reactive oxygen species (Kelly and O'Neill, 2015). This metabolic shift also controls the balance of pro- and anti-inflammatory cytokines, increasing IL-1β and reducing IL-10 (Palsson-McDermott et al., 2015). A recent study revealed a role for the myddosome and the serine threonine kinase TBK1 as upstream signaling components of TLR-inducible glycolysis (Tan and Kagan, 2019). However, other key molecular events connecting macrophage activation to inducible glycolysis and inflammatory responses are poorly understood. Many glycolytic enzymes are regulated by lysine acetylation (Shakespear et al., 2018), and manipulating enzymes that control this post-translational modification represents an exciting strategy for targeting macrophage activation. Here we provide proof of concept for such an approach, demonstrating that class IIa HDACs, especially HDAC7, drive TLR4-induced glycolytic reprogramming and inflammatory responses in macrophages. Mechanistically, we have defined a class IIa HDAC-PKM2 axis that directs the metabolic shift and associated inflammatory responses, and we show that targeting this interaction provides a strategy for selectively manipulating macrophage activation.

Our previous ectopic expression studies in RAW 264.7 murine macrophage-like cells identified a selective role for a specific Hdac7 splice isoform, Hdac7-u, in driving inflammatory gene expression (Shakespear et al., 2013). This isoform lacks the first 22 amino acids and does not bind the transcriptional repressor Ctbp. However, the low levels of *Ctpb* relative to *Hdac7* mRNA in BMMs versus RAW 264.7 cells suggests that this selective role for Hdac7-u may not be apparent in BMMs and other macrophage populations. Indeed, we report here that although Hdac7 has a dominant role, multiple class IIa HDACs interact with PKM2 and contribute to immunometabolism-associated inflammatory responses in both human and mouse macrophages. Of note, the class IIa HDACs, Hdac5 (Poralla et al., 2015) and Hdac9 (Cao et al., 2014), have both been linked to proinflammatory responses in macrophages. Whether HDAC7-u has a selective proinflammatory function in other cell types and/or tissues where Ctbp expression is elevated remains to be addressed.

The rapidly inducible accumulation of glycolytic and TCA cycle metabolites (Jha et al., 2015; Lampropoulou et al., 2016) provide LPS-activated macrophages with biosynthetic intermediates that can also regulate inflammatory responses. A key example

of this is the mitochondrial metabolite succinate, which promotes Il-1β and limits Il-10 (Mills et al., 2016). Consistent with other reports (Tannahill et al., 2013; Jha et al., 2015; Palsson-McDermott et al., 2015; Lampropoulou et al., 2016), we also observed that treatment with LPS increased succinate levels, but TMP269 had no effect on this response. Given that most of the LPS-inducible glycolytic intermediates were reduced by TMP269, our results imply that class IIa HDACs selectively drive glycolysis in macrophages, without a pronounced effect on TCA cycle remodeling. This is also consistent with the more prominent effect of genetic or pharmacological targeting of Hdac7 on LPS-regulated ECAR versus OCR. In line with this, Hdac7 did not regulate LPS-inducible production of NO, which is responsible for TLR-mediated repression of oxidative phosphorylation (OXPHOS) in activated macrophages (Baseler et al., 2016). Although PKM2 has emerged as a key regulator of innate immune cell metabolism and activation through its ability to alter its conformation and associate with transcription factors (Palsson-McDermott et al., 2015), the molecular mechanisms by which it regulates macrophage activation are still poorly understood. Our findings reveal that class IIa HDACs, particularly Hdac7, are essential to this process.

Previous reports in other cell systems have shown that regulated Pkm2 acetylation influences its functions (Lv et al., 2011; Lv et al., 2013). Deacetylation of Pkm2 at K89 was considered as the most likely mechanism by which Hdac7 licenses its inflammatory functions, given that this residue could only be detected in an acetylated form after class IIa HDAC inhibition. Unexpectedly, however, deacetylation of this residue had no apparent role in regulating Il-1β. Instead, deacetylation of Pkm2-specific K433 appears to be critical for promoting expression of this cytokine. Remarkably, a K433 acetyl-dead mutant of Pkm2 was hyperactive in driving Il-1β and was insensitive to class IIa HDAC inhibition, thus demonstrating a key requirement for K433 deacetylation in driving macrophage inflammatory responses. Acetylation of PKM2 at K433 by p300 acetyltransferase inhibited the PK activity of PKM2 by reducing affinity for the allosteric activator fructose 1,6-bisphosphate (Lv et al., 2013). Thus, Hdac7-mediated enhancement of Pkm2 PK activity that we observed may be a consequence of K433 deacetylation. Interestingly, we found that PK activity was elevated in LPS-activated macrophages and that this response was class IIa HDAC dependent. Our findings thus challenge the view that PKM2 PK activity is suppressed in activated macrophages to enable it to drive inflammatory responses. Rather, our data support a model in which class IIa HDAC-mediated deacetylation of Pkm2 licenses both its glycolytic and inflammatory functions.

Given that both Hdac7 and Pkm2 can interact with Hif1α (Shakespear et al., 2013; Palsson-McDermott et al., 2015), it is likely that these three proteins act as part of a complex to control macrophage inflammatory responses. A landmark study in the immunometabolism field showed that LPS induces a switch to the dimeric form of PKM2, which then localizes to the nucleus in macrophages (Palsson-McDermott et al., 2015). This effect was linked to Hif1α-mediated glycolytic and inflammatory gene expression. Under our conditions, we did not observe the appearance of dimeric Pkm2 in the nucleus after LPS stimulation. We thus conclude that although it may have additional nuclear functions in macrophages, dimeric Pkm2 most likely acts in the cytoplasm to drive inflammatory responses. Of note, a previous study showed that cytoplasmic, dimeric PKM2 acted as a co-chaperone to regulate EGFR half-life in lung cancer cells (Yang et al., 2016). Interestingly, nuclear PKM2 was observed in monocytes and macrophages from patients with coronary artery disease, with this resulting in PKM2-mediated STAT3 activation (Shirai et al., 2016). Whether class IIa HDACs influence the PKM2-STAT3 pathway in this setting warrants further investigation.

Our observation that class IIa HDAC inhibition reduced both cytoplasmic dimeric Pkm2 and nuclear Hif1α suggests that the cytoplasmic Hdac7-Pkm2 complex may stabilize and/or promote Hif1α nuclear translocation. We found that TMP269 interfered with the interaction between Pkm2 and Hif1α, but not Hdac7 and Hif1α. Given that we also found that Hdac7 and Pkm2 directly interact, the most likely explanation for these observations is that the interaction between Hdac7 and Hif1α is direct, whereas that of Pkm2 and Hif1α is indirect. In this scenario, disrupting the Hdac7/Pkm2 complex would be predicted to have the effects described above. Nonetheless, how Hdac7-mediated deacetylation of Pkm2 regulates Hif1α function remains to be determined. This transcription factor can itself be regulated by deacetylation (Geng et al., 2011), so HDAC7-mediated PKM2 deacetylation might enable a subsequent modification of HIF1α, permitting its stabilization and/or nuclear translocation. Another possibility is that in macrophages, the K433 acetylated form of PKM2, as part of a larger complex with HDAC7 and possibly other proteins, indirectly interacts with HIF1α to retain it in the cytoplasm for degradation. Class IIa HDAC-mediated deacetylation at K433 might thus enable its release and nuclear translocation.

Anti-inflammatory effects of broad-spectrum HDACi have been observed in multiple inflammation models in mice (Halili et al., 2009; Shakespear et al., 2011). Here we show that selective inhibition of class IIa HDAC enzymes suppresses LPS-induced systemic inflammatory responses and Il-1β levels *in vivo*. The fact that class IIa HDAC inhibition antagonized Pkm2-mediated inflammatory responses may be important, given that PKM2 has itself long been pursued as a target in cancer (Dayton et al., 2016) and more recently in inflammation (Alves-Filho and Pålsson-McDermott, 2016). Extended treatment with an inhibitor of class IIa HDAC enzymes reduced tumor burdens and metastasis in mouse breast cancer models, with these effects being linked to an immunostimulatory tumor-associated macrophage phenotype (Guerriero et al., 2017). Our findings raise the possibility that inhibiting PKM2 function might also contribute to this anti-tumor activity.

Variation in HDAC7 expression has been associated with inflammation-related diseases, including systemic sclerosis (Hemmatazad et al., 2009), primary sclerosing cholangitis (Liu et al., 2013), colorectal cancer (Stypula-Cyrus et al., 2013; Gerçeker et al., 2015; Kasap et al., 2016), and B cell malignancies (Barneda-Zahonero et al., 2015). An HDAC7 variant was also recently linked to early-onset systemic lupus erythematosus (Batu et al., 2018). Detailed profiling of class IIa HDAC enzymes across inflammation-mediated disease models is thus expected to reveal specific inflammatory diseases for which inhibitors of

class IIa HDAC enzymes may be efficacious. It certainly seems plausible that treatment with class IIa HDACi to selectively inhibit IL-1β and CCL2, but amplify IL-10, might suppress both myeloid cell infiltration and activation in the context of inflammatory diseases.

Advances in understanding metabolic control of innate immunity have led to exciting possibilities for ameliorating inflammation-driven pathology. For example, TCA cycle-derived citrate is converted into itaconic acid that suppresses macrophage inflammatory responses, a phenomenon exploited for the development of an anti-inflammatory itaconate derivative (Mills et al., 2018). Moreover, the immunomodulatory drug dimethyl fumarate was recently shown to exert its anti-inflammatory effects by targeting GAPDH to disrupt glycolysis (Kornberg et al., 2018). Of note, we found that Hdac7 also interacts with Gapdh in macrophages, so it is possible that class IIa HDACs also regulate macrophage metabolism and inflammatory responses via this interaction. The majority of glycolytic and TCA cycle enzymes are regulated by lysine acetylation (Choudhary et al., 2014), and our study demonstrates that it is possible to pharmacologically target glycolysis in macrophages using a sub-class of HDACs that have, as yet, been underexplored in drug discovery applications. Class IIa HDAC family members may operate in similar ways in other cell populations where regulated cell metabolism enables specific functional responses, for example, during T cell activation and cancer cell proliferation. Pharmacological targeting of the class IIa HDAC-PKM2 signaling axis may thus have applications in modulating inflammation-driven conditions.

STAR★METHODS

Detailed methods are provided in the online version of this paper and include the following:

- KEY RESOURCES TABLE
- LEAD CONTACT AND MATERIALS AVAILABILITY
- EXPERIMENTAL MODELS
  - Animals
  - Primary cell cultures
  - Cell lines
  - Ethics statement
- METHOD DETAILS
  - Preparation of HDAC inhibitors
  - Generation of Hdac7 mutant (Hdac7ΔH649A) and molecular modeling
  - Generation of Pkm2 point mutants (K89R, K305R, K433R)
  - Retroviral transduction
  - Gene silencing
  - Cytokine analysis
  - Estimation of nitric oxide
  - Protein lysates and immunoblotting
  - Size exclusion chromatography
  - Co-immunoprecipitation
  - Gene expression analyses
  - Proximity ligation assay/immunofluorescence
  - Measurement of pyruvate kinase (PK) activity
  - Metabolic flux analysis
  - Glucose uptake by 2-NBDG
  - Measurement of extracellular lactate
  - Class IIa HDAC enzyme assay
  - Rapid immunoprecipitation mass spectrometry of endogenous proteins (RIME)
  - Mass spectrometric identification of acetylated lysine residues
  - Metabolic profiling of LPS-activated macrophages
  - Cell-free protein expression using the Leishmania tarentolae system and protein-protein interaction studies by AlphaLISA assays
  - Cell death quantification
  - LPS-induced inflammation model
- QUANTIFICATION AND STATISTICAL ANALYSIS
- DATA AND CODE AVAILABILITY

SUPPLEMENTAL INFORMATION

Supplemental Information can be found online at https://doi.org/10.1016/j.celrep.2020.02.007.

ACKNOWLEDGMENTS

This work was supported by a project grant (APP1047921) and an ideas grant (APP1184885) from the National Health and Medical Research Council (NHMRC) of Australia and an Australian Research Council Discovery Project (DP170102321). M.R.S. was supported by a University of Queensland Postdoctoral Fellowship. M.J.S. (APP1107914) and B.M.C. (APP1136021) are supported by NHMRC Senior Research Fellowships. D.P.F. is supported by NHMRC Senior Principal Research Fellowships (APP1027369 and APP1117017). K.A. is supported by an Australian Research Council (ARC) linkage project (LP150100689), an NHMRC program grant (APP1037320), and a CSIRO Future Science platform in synthetic biology. A.I. is supported by a University of Queensland Postdoctoral Fellowship and a University of Queensland Early Career Grant. L.L. is supported by an ARC Discovery Early Career Researcher Award (DECRA; DE180100524). We acknowledge the support of the Institute for Molecular Bioscience Dynamic Imaging Facility for Cancer Biology at The University of Queensland, established with the support of the Australian Cancer Research Foundation; the IMB Mass Spectrometry Facility; the Transgenic Animal Facility of Queensland (a division of The University of Queensland Biological Resources Department); and the ARC Centre of Excellence in Advanced Molecular Imaging (CE140100011). Metabolomics Australia is part of the Bioplatforms Australia network, funded through the Australian Government's National Collaborative Research Infrastructure Strategy (NCRIS). We thank Prof. Eric Olson and Dr. Rhonda Bassel-Duby for providing *HDAC7*$^{fl/fl}$ mice (UT Southwestern Medical Center), the Australian Red Cross Blood Service for providing buffy coats used in these studies, and Prof. Alpha Yap (IMB, The University of Queensland) for critical review of the manuscript.

AUTHOR CONTRIBUTIONS

Conceptualization, M.R.S., K.D.G., A.I., D.P.F., and M.J.S.; Methodology, M.R.S., K.D.G., and M.J.S.; Formal Analysis, W.X.; Investigation, K.D.G., M.R.S., J.E.B.C., A.I., D.R., A.M.V.M., M.P.H., V.A.T., J.B.v.P., K.T., T.K., J.H.G., D.M.H., G.M.K., A.J.S., S.V.M., W.A.J., L.L., and A.J.; Resources, R.C.R.; Writing – Original Draft, K.D.G., M.R.S., and M.J.S.; Writing – Review & Editing, M.R.S., K.D.G., A.I., D.R., M.P.H., L.L., D.P.F., and M.J.S.; Supervision, M.R.S., W.J., K.A., B.M.C., A.B., J.L.S., D.P.F., and M.J.S.; Funding Acquisition, D.P.F. and M.J.S.

DECLARATION OF INTERESTS

The authors declare no competing interests.

Received: November 13, 2018
Revised: September 30, 2019
Accepted: February 3, 2020
Published: February 25, 2020

REFERENCES

Allfrey, V.G., Faulkner, R., and Mirsky, A.E. (1964). Acetylation and methylation of histones and their possible role in the regulation of RNA synthesis. Proc. Natl. Acad. Sci. U S A *51*, 786–794.

Alves-Filho, J.C., and Pålsson-McDermott, E.M. (2016). Pyruvate kinase M2: a potential target for regulating inflammation. Front. Immunol. *7*, 145.

Anastasiou, D., Yu, Y., Israelsen, W.J., Jiang, J.K., Boxer, M.B., Hong, B.S., Tempel, W., Dimov, S., Shen, M., Jha, A., et al. (2012). Pyruvate kinase M2 activators promote tetramer formation and suppress tumorigenesis. Nat. Chem. Biol. *8*, 839–847.

Ashburner, B.P., Westerheide, S.D., and Baldwin, A.S., Jr. (2001). The p65 (RelA) subunit of NF-kappaB interacts with the histone deacetylase (HDAC) corepressors HDAC1 and HDAC2 to negatively regulate gene expression. Mol. Cell. Biol. *21*, 7065–7077.

Aung, H.T., Schroder, K., Himes, S.R., Brion, K., van Zuylen, W., Trieu, A., Suzuki, H., Hayashizaki, Y., Hume, D.A., Sweet, M.J., and Ravasi, T. (2006). LPS regulates proinflammatory gene expression in macrophages by altering histone deacetylase expression. FASEB J. *20*, 1315–1327.

Barneda-Zahonero, B., Collazo, O., Azagra, A., Fernández-Duran, I., Serra-Musach, J., Islam, A.B., Vega-García, N., Malatesta, R., Camós, M., Gómez, A., et al. (2015). The transcriptional repressor HDAC7 promotes apoptosis and c-Myc downregulation in particular types of leukemia and lymphoma. Cell Death Dis. *6*, e1635.

Baseler, W.A., Davies, L.C., Quigley, L., Ridnour, L.A., Weiss, J.M., Hussain, S.P., Wink, D.A., and McVicar, D.W. (2016). Autocrine IL-10 functions as a rheostat for M1 macrophage glycolytic commitment by tuning nitric oxide production. Redox Biol. *10*, 12–23.

Batu, E.D., Koşukcu, C., Taşkıran, E., Sahin, S., Akman, S., Sözeri, B., Ünsal, E., Bilginer, Y., Kasapcopur, O., Alikaşifoğlu, M., and Ozen, S. (2018). Whole exome sequencing in early-onset systemic lupus erythematosus. J. Rheumatol. *45*, 1671–1679.

Brogdon, J.L., Xu, Y., Szabo, S.J., An, S., Buxton, F., Cohen, D., and Huang, Q. (2007). Histone deacetylase activities are required for innate immune cell control of Th1 but not Th2 effector cell function. Blood *109*, 1123–1130.

Cao, Q., Rong, S., Repa, J.J., St Clair, R., Parks, J.S., and Mishra, N. (2014). Histone deacetylase 9 represses cholesterol efflux and alternatively activated macrophages in atherosclerosis development. Arterioscler. Thromb. Vasc. Biol. *34*, 1871–1879.

Chang, S., Young, B.D., Li, S., Qi, X., Richardson, J.A., and Olson, E.N. (2006). Histone deacetylase 7 maintains vascular integrity by repressing matrix metalloproteinase 10. Cell *126*, 321–334.

Chatterjee, T.K., Idelman, G., Blanco, V., Blomkalns, A.L., Piegore, M.G., Jr., Weintraub, D.S., Kumar, S., Rajsheker, S., Manka, D., Rudich, S.M., et al. (2011). Histone deacetylase 9 is a negative regulator of adipogenic differentiation. J. Biol. Chem. *286*, 27836–27847.

Choudhary, C., Kumar, C., Gnad, F., Nielsen, M.L., Rehman, M., Walther, T.C., Olsen, J.V., and Mann, M. (2009). Lysine acetylation targets protein complexes and co-regulates major cellular functions. Science *325*, 834–840.

Choudhary, C., Weinert, B.T., Nishida, Y., Verdin, E., and Mann, M. (2014). The growing landscape of lysine acetylation links metabolism and cell signalling. Nat. Rev. Mol. Cell Biol. *15*, 536–550.

Das Gupta, K., Shakespear, M.R., Iyer, A., Fairlie, D.P., and Sweet, M.J. (2016). Histone deacetylases in monocyte/macrophage development, activation and metabolism: refining HDAC targets for inflammatory and infectious diseases. Clin. Transl. Immunology *5*, e62.

Dayton, T.L., Jacks, T., and Vander Heiden, M.G. (2016). PKM2, cancer metabolism, and the road ahead. EMBO Rep. *17*, 1721–1730.

Falkenberg, K.J., and Johnstone, R.W. (2014). Histone deacetylases and their inhibitors in cancer, neurological diseases and immune disorders. Nat. Rev. Drug Discov. *13*, 673–691.

Fischle, W., Dequiedt, F., Hendzel, M.J., Guenther, M.G., Lazar, M.A., Voelter, W., and Verdin, E. (2002). Enzymatic activity associated with class II HDACs is dependent on a multiprotein complex containing HDAC3 and SMRT/N-CoR. Mol. Cell *9*, 45–57.

Gaber, T., Strehl, C., and Buttgereit, F. (2017). Metabolic regulation of inflammation. Nat. Rev. Rheumatol. *13*, 267–279.

Gagoski, D., Mureev, S., Giles, N., Johnston, W., Dahmer-Heath, M., Škalamera, D., Gonda, T.J., and Alexandrov, K. (2015). Gateway-compatible vectors for high-throughput protein expression in pro- and eukaryotic cell-free systems. J. Biotechnol. *195*, 1–7.

Geng, H., Harvey, C.T., Pittsenbarger, J., Liu, Q., Beer, T.M., Xue, C., and Qian, D.Z. (2011). HDAC4 protein regulates HIF1α protein lysine acetylation and cancer cell response to hypoxia. J. Biol. Chem. *286*, 38095–38102.

Gerçeker, E., Boyacıoglu, S.O., Kasap, E., Baykan, A., Yuceyar, H., Yıldırım, H., Ayhan, S., Ellidokuz, E., and Korkmaz, M. (2015). Never in mitosis gene A-related kinase 6 and aurora kinase A: New gene biomarkers in the conversion from ulcerative colitis to colorectal cancer. Oncol. Rep. *34*, 1905–1914.

Guerriero, J.L., Sotayo, A., Ponichtera, H.E., Castrillon, J.A., Pourzia, A.L., Schad, S., Johnson, S.F., Carrasco, R.D., Lazo, S., Bronson, R.T., et al. (2017). Class IIa HDAC inhibition reduces breast tumours and metastases through anti-tumour macrophages. Nature *543*, 428–432.

Halili, M.A., Andrews, M.R., Sweet, M.J., and Fairlie, D.P. (2009). Histone deacetylase inhibitors in inflammatory disease. Curr. Top. Med. Chem. *9*, 309–319.

Halili, M.A., Andrews, M.R., Labzin, L.I., Schroder, K., Matthias, G., Cao, C., Lovelace, E., Reid, R.C., Le, G.T., Hume, D.A., et al. (2010). Differential effects of selective HDAC inhibitors on macrophage inflammatory responses to the Toll-like receptor 4 agonist LPS. J. Leukoc. Biol. *87*, 1103–1114.

Hemmatazad, H., Rodrigues, H.M., Maurer, B., Brentano, F., Pileckyte, M., Distler, J.H., Gay, R.E., Michel, B.A., Gay, S., Huber, L.C., et al. (2009). Histone deacetylase 7, a potential target for the antifibrotic treatment of systemic sclerosis. Arthritis Rheum. *60*, 1519–1529.

Hsu, K.C., Liu, C.Y., Lin, T.E., Hsieh, J.H., Sung, T.Y., Tseng, H.J., Yang, J.M., and Huang, W.J. (2017). Novel class IIa-selective histone deacetylase inhibitors discovered using an in silico virtual screening approach. Sci. Rep. *7*, 3228.

Jha, A.K., Huang, S.C., Sergushichev, A., Lampropoulou, V., Ivanova, Y., Loginicheva, E., Chmielewski, K., Stewart, K.M., Ashall, J., Everts, B., et al. (2015). Network integration of parallel metabolic and transcriptional data reveals metabolic modules that regulate macrophage polarization. Immunity *42*, 419–430.

Johnston, W.A., and Alexandrov, K. (2014). Production of eukaryotic cell-free lysate from Leishmania tarentolae. Methods Mol. Biol. *1118*, 1–15.

Kasap, E., Gerceker, E., Boyacıoglu, S.O., Yuceyar, H., Yıldırm, H., Ayhan, S., and Korkmaz, M. (2016). The potential role of the NEK6, AURKA, AURKB, and PAK1 genes in adenomatous colorectal polyps and colorectal adenocarcinoma. Tumour Biol. *37*, 3071–3080.

Kelly, B., and O'Neill, L.A. (2015). Metabolic reprogramming in macrophages and dendritic cells in innate immunity. Cell Res. *25*, 771–784.

Kornberg, M.D., Bhargava, P., Kim, P.M., Putluri, V., Snowman, A.M., Putluri, N., Calabresi, P.A., and Snyder, S.H. (2018). Dimethyl fumarate targets GAPDH and aerobic glycolysis to modulate immunity. Science *360*, 449–453.

Kovtun, O., Mureev, S., Jung, W., Kubala, M.H., Johnston, W., and Alexandrov, K. (2011). Leishmania cell-free protein expression system. Methods *55*, 58–64.

Lampropoulou, V., Sergushichev, A., Bambouskova, M., Nair, S., Vincent, E.E., Loginicheva, E., Cervantes-Barragan, L., Ma, X., Huang, S.C., Griss, T., et al. (2016). Itaconate links inhibition of succinate dehydrogenase with macrophage metabolic remodeling and regulation of inflammation. Cell Metab. *24*, 158–166.

Lee, Y.L., Lin, S.K., Hou, K.L., Kok, S.H., Lai, E.H., Wang, H.W., Chang, J.Z., Yang, H., and Hong, C.Y. (2018). Sirtuin 6 attenuates periapical lesion propagation by modulating hypoxia-induced chemokine (C-C motif) ligand 2 production in osteoblasts. Int. Endod. J. *51* (*Suppl 2*), e74–e86.

Liu, J.Z., Hov, J.R., Folseraas, T., Ellinghaus, E., Rushbrook, S.M., Doncheva, N.T., Andreassen, O.A., Weersma, R.K., Weismüller, T.J., Eksteen, B., et al.; UK-PSCSC Consortium; International PSC Study Group; International IBD Genetics Consortium (2013). Dense genotyping of immune-related disease regions identifies nine new risk loci for primary sclerosing cholangitis. Nat. Genet. *45*, 670–675.

Livak, K.J., and Schmittgen, T.D. (2001). Analysis of relative gene expression data using real-time quantitative PCR and the 2(-Delta delta C(T)) method. Methods *25*, 402–408.

Lobera, M., Madauss, K.P., Pohlhaus, D.T., Wright, Q.G., Trocha, M., Schmidt, D.R., Baloglu, E., Trump, R.P., Head, M.S., Hofmann, G.A., et al. (2013). Selective class IIa histone deacetylase inhibition via a nonchelating zinc-binding group. Nat. Chem. Biol. *9*, 319–325.

Lv, L., Li, D., Zhao, D., Lin, R., Chu, Y., Zhang, H., Zha, Z., Liu, Y., Li, Z., Xu, Y., et al. (2011). Acetylation targets the M2 isoform of pyruvate kinase for degradation through chaperone-mediated autophagy and promotes tumor growth. Mol. Cell *42*, 719–730.

Lv, L., Xu, Y.P., Zhao, D., Li, F.L., Wang, W., Sasaki, N., Jiang, Y., Zhou, X., Li, T.T., Guan, K.L., et al. (2013). Mitogenic and oncogenic stimulation of K433 acetylation promotes PKM2 protein kinase activity and nuclear localization. Mol. Cell *52*, 340–352.

Ma, C., and D'Mello, S.R. (2011). Neuroprotection by histone deacetylase-7 (HDAC7) occurs by inhibition of c-jun expression through a deacetylase-independent mechanism. J. Biol. Chem. *286*, 4819–4828.

Margariti, A., Zampetaki, A., Xiao, Q., Zhou, B., Karamariti, E., Martin, D., Yin, X., Mayr, M., Li, H., Zhang, Z., et al. (2010). Histone deacetylase 7 controls endothelial cell growth through modulation of beta-catenin. Circ. Res. *106*, 1202–1211.

Martin, M., Kettmann, R., and Dequiedt, F. (2007). Class IIa histone deacetylases: regulating the regulators. Oncogene *26*, 5450–5467.

McDonald, T.S., Tan, K.N., Hodson, M.P., and Borges, K. (2014). Alterations of hippocampal glucose metabolism by even versus uneven medium chain triglycerides. J. Cereb. Blood Flow Metab. *34*, 153–160.

Medina-Torres, C.E., van Eps, A.W., Nielsen, L.K., and Hodson, M.P. (2015). A liquid chromatography-tandem mass spectrometry-based investigation of the lamellar interstitial metabolome in healthy horses and during experimental laminitis induction. Vet. J. *206*, 161–169.

Mihaylova, M.M., Vasquez, D.S., Ravnskjaer, K., Denechaud, P.D., Yu, R.T., Alvarez, J.G., Downes, M., Evans, R.M., Montminy, M., and Shaw, R.J. (2011). Class IIa histone deacetylases are hormone-activated regulators of FOXO and mammalian glucose homeostasis. Cell *145*, 607–621.

Mills, E.L., Kelly, B., Logan, A., Costa, A.S.H., Varma, M., Bryant, C.E., Tourlomousis, P., Dabritz, J.H.M., Gottlieb, E., Latorre, I., et al. (2016). Succinate dehydrogenase supports metabolic repurposing of mitochondria to drive inflammatory macrophages. Cell *167*, 457–470.e13.

Mills, E.L., Ryan, D.G., Prag, H.A., Dikovskaya, D., Menon, D., Zaslona, Z., Jedrychowski, M.P., Costa, A.S.H., Higgins, M., Hams, E., et al. (2018). Itaconate is an anti-inflammatory metabolite that activates Nrf2 via alkylation of KEAP1. Nature *556*, 113–117.

Mohammed, H., Taylor, C., Brown, G.D., Papachristou, E.K., Carroll, J.S., and D'Santos, C.S. (2016). Rapid immunoprecipitation mass spectrometry of endogenous proteins (RIME) for analysis of chromatin complexes. Nat. Protoc. *11*, 316–326.

Morita, S., Kojima, T., and Kitamura, T. (2000). Plat-E: an efficient and stable system for transient packaging of retroviruses. Gene Ther. *7*, 1063–1066.

O'Neill, L.A., and Pearce, E.J. (2016). Immunometabolism governs dendritic cell and macrophage function. J. Exp. Med. *213*, 15–23.

O'Neill, L.A., Golenbock, D., and Bowie, A.G. (2013). The history of Toll-like receptors—redefining innate immunity. Nat. Rev. Immunol. *13*, 453–460.

Ovchinnikov, D.A., van Zuylen, W.J., DeBats, C.E., Alexander, K.A., Kellie, S., and Hume, D.A. (2008). Expression of Gal4-dependent transgenes in cells of the mononuclear phagocyte system labeled with enhanced cyan fluorescent protein using Csf1r-Gal4VP16/UAS-ECFP double-transgenic mice. J. Leukoc. Biol. *83*, 430–433.

Palsson-McDermott, E.M., Curtis, A.M., Goel, G., Lauterbach, M.A., Sheedy, F.J., Gleeson, L.E., van den Bosch, M.W., Quinn, S.R., Domingo-Fernandez, R., Johnston, D.G., et al. (2015). Pyruvate kinase M2 regulates Hif-1α activity and IL-1β induction and is a critical determinant of the warburg effect in LPS-activated macrophages. Cell Metab. *21*, 65–80.

PerkinElmer (2016). Anti-GFP AlphaLISA protocol (Perkin Elmer). https://www.perkinelmer.com/lab-solutions/resources/docs/009625A_01_GDE.pdf.

Poralla, L., Stroh, T., Erben, U., Sittig, M., Liebig, S., Siegmund, B., and Glauben, R. (2015). Histone deacetylase 5 regulates the inflammatory response of macrophages. J. Cell. Mol. Med. *19*, 2162–2171.

Prakasam, G., Iqbal, M.A., Bamezai, R.N.K., and Mazurek, S. (2018). Post-translational modifications of pyruvate kinase M2: tweaks that benefit cancer. Front. Oncol. *8*, 22.

Roger, T., Lugrin, J., Le Roy, D., Goy, G., Mombelli, M., Koessler, T., Ding, X.C., Chanson, A.L., Reymond, M.K., Miconnet, I., et al. (2011). Histone deacetylase inhibitors impair innate immune responses to Toll-like receptor agonists and to infection. Blood *117*, 1205–1217.

Rossol, M., Heine, H., Meusch, U., Quandt, D., Klein, C., Sweet, M.J., and Hauschildt, S. (2011). LPS-induced cytokine production in human monocytes and macrophages. Crit. Rev. Immunol. *31*, 379–446.

Sadler, A.J., Rossello, F.J., Yu, L., Deane, J.A., Yuan, X., Wang, D., Irving, A.T., Kaparakis-Liaskos, M., Gantier, M.P., Ying, H., et al. (2015). BTB-ZF transcriptional regulator PLZF modifies chromatin to restrain inflammatory signaling programs. Proc. Natl. Acad. Sci. USA *112*, 1535–1540.

Sauter, K.A., Pridans, C., Sehgal, A., Bain, C.C., Scott, C., Moffat, L., Rojo, R., Stutchfield, B.M., Davies, C.L., Donaldson, D.S., et al. (2014). The MacBlue binary transgene (csf1r-gal4VP16/UAS-ECFP) provides a novel marker for visualisation of subsets of monocytes, macrophages and dendritic cells and responsiveness to CSF1 administration. PLoS ONE *9*, e105429.

Schlumm, F., Mauceri, D., Freitag, H.E., and Bading, H. (2013). Nuclear calcium signaling regulates nuclear export of a subset of class IIa histone deacetylases following synaptic activity. J. Biol. Chem. *288*, 8074–8084.

Shakespear, M.R., Halili, M.A., Irvine, K.M., Fairlie, D.P., and Sweet, M.J. (2011). Histone deacetylases as regulators of inflammation and immunity. Trends Immunol. *32*, 335–343.

Shakespear, M.R., Hohenhaus, D.M., Kelly, G.M., Kamal, N.A., Gupta, P., Labzin, L.I., Schroder, K., Garceau, V., Barbero, S., Iyer, A., et al. (2013). Histone deacetylase 7 promotes Toll-like receptor 4-dependent proinflammatory gene expression in macrophages. J. Biol. Chem. *288*, 25362–25374.

Shakespear, M.R., Iyer, A., Cheng, C.Y., Das Gupta, K., Singhal, A., Fairlie, D.P., and Sweet, M.J. (2018). Lysine deacetylases and regulated glycolysis in macrophages. Trends Immunol. *39*, 473–488.

Shirai, T., Nazarewicz, R.R., Wallis, B.B., Yanes, R.E., Watanabe, R., Hilhorst, M., Tian, L., Harrison, D.G., Giacomini, J.C., Assimes, T.L., et al. (2016). The glycolytic enzyme PKM2 bridges metabolic and inflammatory dysfunction in coronary artery disease. J. Exp. Med. *213*, 337–354.

Stypula-Cyrus, Y., Damania, D., Kunte, D.P., Cruz, M.D., Subramanian, H., Roy, H.K., and Backman, V. (2013). HDAC up-regulation in early colon field carcinogenesis is involved in cell tumorigenicity through regulation of chromatin structure. PLoS ONE *8*, e64600.

Takenaka, M., Noguchi, T., Sadahiro, S., Hirai, H., Yamada, K., Matsuda, T., Imai, E., and Tanaka, T. (1991). Isolation and characterization of the human pyruvate kinase M gene. Eur. J. Biochem. *198*, 101–106.

Tan, Y., and Kagan, J.C. (2019). Innate immune signaling organelles display natural and programmable signaling flexibility. Cell *177*, 384–398.e11.

Tannahill, G.M., Curtis, A.M., Adamik, J., Palsson-McDermott, E.M., McGettrick, A.F., Goel, G., Frezza, C., Bernard, N.J., Kelly, B., Foley, N.H., et al. (2013). Succinate is an inflammatory signal that induces IL-1β through HIF-1α. Nature *496*, 238–242.

Yan, B., Xie, S., Liu, Z., Ran, J., Li, Y., Wang, J., Yang, Y., Zhou, J., Li, D., and Liu, M. (2014). HDAC6 deacetylase activity is critical for lipopolysaccharide-induced activation of macrophages. PLoS ONE *9*, e110718.

Yang, L., Xie, M., Yang, M., Yu, Y., Zhu, S., Hou, W., Kang, R., Lotze, M.T., Billiar, T.R., Wang, H., et al. (2014). PKM2 regulates the Warburg effect and promotes HMGB1 release in sepsis. Nat. Commun. *5*, 4436.

Yang, Y.C., Cheng, T.Y., Huang, S.M., Su, C.Y., Yang, P.W., Lee, J.M., Chen, C.K., Hsiao, M., Hua, K.T., and Kuo, M.L. (2016). Cytosolic PKM2 stabilizes mutant EGFR protein expression through regulating HSP90-EGFR association. Oncogene *35*, 3387–3398.

Youn, G.S., Lee, K.W., Choi, S.Y., and Park, J. (2016). Overexpression of HDAC6 induces pro-inflammatory responses by regulating ROS-MAPK-NF-κB/AP-1 signaling pathways in macrophages. Free Radic. Biol. Med. *97*, 14–23.

Zhang, X., and Mosser, D.M. (2008). Macrophage activation by endogenous danger signals. J. Pathol. *214*, 161–178.

STAR★METHODS

KEY RESOURCES TABLE

REAGENT or RESOURCE	SOURCE	IDENTIFIER
Antibodies		
HDAC7 (D4E1L)	Cell Signaling Technology	Cat#33418; RRID: AB_2716756
HDAC4/5/7	Santa Cruz Biotechnology	Sc-11421; RRID: AB_647888
Histone H3	Cell Signaling Technology	Cat#3638S; RRID: AB_1642229
IL-1β	R&D Systems	AF-401-NA; RRID: AB_416684
p38	Cell Signaling Technology	Cat#8690S; RRID: AB_ 10999090
Tubulin	Sigma Aldrich	Cat#T5168; RRID: AB_477579
V5	Bio-Rad/AbD Serotec	MCA1360; RRID: AB_322378
FLAG	Sigma Aldrich	F7425; RRID: AB_439687
PKM2	Cell Signaling Technology	Cat#3198; RRID: AB_2252325
S6	Cell Signaling Technology	Cat#2217; RRID: AB_331355
HIF1α	Novus	NB100-449; RRID: AB_10001045
Lamin A/C	Cell Signaling Technology	Cat#2032S; RRID: AB_ 2136278
pPKM2 Y105	Cell Signaling Technology	Cat#3827; RRID: AB_1950369
Acetyl lysine	Cell Signaling Technology	Cat#9441S; RRID: AB_ 331805
Alexa Fluor 647	Thermo Fisher Scientific	A21443, RRID: AB_1500685
Chemicals, Peptides, and Recombinant Proteins		
Lipopolysaccharide	Sigma Aldrich	L2137
2-Deoxy-D-glucose (2-DG)	Sigma Aldrich	D8375, CAS 154-17-6
2-NBDG	Thermo Fisher Scientific	N3195
Tubastatin A	Sigma Aldrich	SML0044
HIF1α inhibitor	Santa Cruz Biotechnology	CAS 934593-90-5
DASA	Calbiochem	Cat#550602
Recombinant human CSF-1	Chiron	N/A
PMA	Sigma Aldrich	P1585
Lipofectamine 2000	Thermo Fisher Scientific	11668019
Polybrene	Merck	TR-1003-G
Recombinant human IFNγ	R&D Systems	285-IF
Nigericin	Sigma Aldrich	N7143
Critical Commercial Assays		
Legendplex	BioLegend	Cat#740150
Mito Stress Test Kit	Seahorse Bioscience	103015-100
L-Lactate assay kit	Abcam	ab65331
LDH cytotoxicity assay kit	Promega	G1780
Griess Reagent	Promega	TB229
Duolink *In situ* Detection Reagents Orange	Sigma Aldrich	DUO92007
Pyruvate kinase activity assay kit	Abcam	ab83432
Human IL-1β ELISA kit	R&D Systems	DY201
Human MCP-1 (CCL2) ELISA kit	eBiosciences	88-7399-76
Human TNF ELISA kit	Peprotech	900-K25
Mouse IL-1β ELISA kit	eBiosciences	88-7013-77
Mouse TNF ELISA kit	BD OptEIA	558534
Mouse CCL2 ELISA kit	eBiosciences	88-7391-77
Mouse IL-10 ELISA kit	BD OptEIA	555252
Mouse IL-12p40 ELISA kit	BD OptEIA	555256

(*Continued on next page*)

Continued

REAGENT or RESOURCE	SOURCE	IDENTIFIER
Experimental Models: Cell Lines		
HEK293T	ATCC	CRL-3216
PlatE	CELL BIOLABS, INC	RV-101
THP-1	ATCC	TIB-202
RAW264.7	ATCC	SC-6003
Experimental Models: Organisms/Strains		
C57BL/6J	In-house breeding colony	N/A
MacBlue	In-house breeding colony	N/A
UAS-Hdac7	This paper	N/A
Mac-Hdac7	This paper	N/A
$Hdac7^{flox/flox}$	Obtained from Prof. Eric Olson's lab – UT South Western Medical Centre	N/A
$LysM^{Cre}$	In-house breeding colony	N/A
$Hdac7^{flox/flox}xLysM^{Cre}$	This paper	N/A
Oligonucleotides		
Real time primer for mouse *Il1b* Fwd: AACCAACAAGT GATATTCTCC	This paper	N/A
Real time primer for mouse *Il1b* Rev: GATCCACACTC TCCAGCTGCA	This paper	N/A
Real time primer for mouse *Hdac7* Fwd: CGCAGCCA GTGTGAGTGTCT	This paper	N/A
Real time primer for mouse *Hdac7* Rev: AGTGGGTTC GTGCCGTAGAG	This paper	N/A
Real time primer for human *HDAC7* Fwd: TCAGAGGC GTCACAGATGGC	This paper	N/A
Real time primer for human *HDAC7* Rev: GGATTTGA TGCTGCTGAGGG	This paper	N/A
si-RNA for human *HDAC7* #1- GAGCCCAUGAGGCU CUCCAUGGAC	Life Technologies	HSS147500
si-RNA for human *HDAC7* #2- GCACCCUCAGGUGU UGCUCUGGGA	Life Technologies	HSS147499
si-RNA for human *HDAC7* #3- GAGCCCAACCUGAAG CUGCGCUAU	Life Technologies	HSS147501
si-RNA for mouse *Hdac7* #1- CUGGAUAACGGGAAGCUUA	Dharmacon/Horizon Discovery	L-040703-00-0005
si-RNA for mouse *Hdac7* #2- CGACCUUGCCUUCAAAGUA	Dharmacon/Horizon Discovery	L-040703-00-0005
si-RNA for mouse *Hdac7* #3- GCUACAAACCCAAGAAAUC	Dharmacon/Horizon Discovery	L-040703-00-0005
si-RNA for mouse *Hdac7* #4- GCCCAUUGCCCGAGAGUUU	Dharmacon/Horizon Discovery	L-040703-00-0005
For details of other real time primers and siRNAs used in this study see Table S2		N/A
Recombinant DNA		
pLHCX-FLAG-mPkm2	Addgene	Cat#44239
pEF6-Hdac7-V5	Sweet Laboratory	N/A
pGene-Hdac7-V5	Sweet Laboratory	N/A
pEF6-FLAG-Pkm2	Sweet Laboratory	N/A
pEF6-FLAG-Pkm2-K89R	Sweet Laboratory	N/A
pEF6-FLAG-Pkm2-K305R	Sweet Laboratory	N/A
pEF6-FLAG-Pkm2-K433R	Sweet Laboratory	N/A
pEF6-Hdac7 ΔH649A-V5	Sweet Laboratory	N/A
pEF6-Sox7-V5	Sweet Laboratory	N/A

(*Continued on next page*)

Continued

REAGENT or RESOURCE	SOURCE	IDENTIFIER
pEF6-Hdac6-V5	Sweet Laboratory	N/A
pEF6-Hdac4-V5	Sweet Laboratory	N/A
pEF6-Hdac5-V5	Sweet Laboratory	N/A
pEF6-Hdac9-V5	Sweet Laboratory	N/A
pEF6-Hdac7-FLAG	Sweet Laboratory	N/A
pEF6-Hif-1α-V5	Sweet Laboratory	N/A
pMIGR-Hdac7-V5	Sweet Laboratory	N/A
pMIGR-Hdac7 ΔH649A-V5	Sweet Laboratory	N/A
pMIGR-FLAG-Pkm2	Sweet Laboratory	N/A
pMIGR-FLAG-Pkm2-K89R	Sweet Laboratory	N/A
pMIGR-FLAG-Pkm2-K305R	Sweet Laboratory	N/A
pMIGR-FLAG-Pkm2-K433R	Sweet Laboratory	N/A
pCell-Free_G03-GFP-Pkm2	Alexandrov Laboratory	N/A
pCell-Free_G08-Hdac7(23-504)-mCherry	Alexandrov Laboratory	N/A
pCell-Free_G08-Hdac7(498-938)-mCherry	Alexandrov Laboratory	N/A
Software and Algorithms		
GraphPad Prism 7	GraphPad	https://www.graphpad.com/scientific-software/prism/
Legendplex Data Analysis Software	Biolegend	http://www.vigenetech.com/LEGENDplex7.htm
Seahorse Wave Controller Software	Seahorse Biosciences, Agilent	N/A
Protein Pilot v4.5	ABSciex	N/A
MultiQuant 2.1	ABSciex	N/A
MARS Data Analysis Software	BMG LABTECH	N/A

LEAD CONTACT AND MATERIALS AVAILABILITY

Further information and request for resources and reagents should be directed to and will be fulfilled by the Lead Contact, Matthew J. Sweet (m.sweet@imb.uq.edu.au).

All unique reagents generated in this study are available from the Lead Contact with a completed Materials Transfer Agreement and reasonable compensation by the requestor for their processing and shipping.

EXPERIMENTAL MODELS

Animals

Male and female mice of 8-12 weeks of age were used for this study. C57BL/6J mice were obtained from an in-house breeding colony. MacBlue mice contain two co-inherited transgenes; a modified *c-fms/Csf1r* promoter drives myeloid-restricted expression of the Gal4-VP16 transcriptional activator, which in turn drives Gal4-dependent (upstream activating sequence-containing promoter) expression of cyan fluorescent protein (CFP) (Ovchinnikov et al., 2008). Consequently, these mice express CFP in monocytes and some tissue macrophage populations (Sauter et al., 2014). UAS-Hdac7-u mice were created by pronuclear injection of the pGene-Hdac7-u-V5 construct (splice variant that lacks the first 22 amino acids) into C57BL/6J mice, and these mice were crossed with MacBlue mice. Progeny that inherit both transgenes (Mac-Hdac7 mice) express Hdac7-u in the myeloid compartment, while littermates inheriting one transgene served as experimental control mice. Genotyping primers used for MacBlue mice were: F-GTGCATTGGAACGCGCATTCC and R-GCTGAAGCACTGCACGCCCC; and genotyping primers used for UAS-Hdac7 mice were:

F-GTGCATTGGAACGCGCATTCC and R-AGAGCCTCATGGGCTCGGCTGAGCG. *Hdac7*$^{fl/fl}$ mice, kindly provided by Prof Eric Olson and Dr Rhonda Bassel-Duby (UT Southwestern Medical Centre) (Chang et al., 2006), were crossed with *LysM*^{Cre} mice to generate myeloid-deleted Hdac7 mice on a C57BL/6 background. For all experiments described, *Hdac7*$^{fl/fl}$ littermate control mice were used for comparisons with *Hdac7*$^{fl/fl}$/*LysM*^{Cre} mice. Genotyping primers for *LysM*^{Cre} mice were F-GCATTGCAGACTAGC TAAAGGCAG and R-CCCAGAAATGCCAGATTACG, and those for *Hdac7*$^{fl/fl}$ mice were F-GTTGCAGGGTCAGCAGCGCAGGCTCTG and R- CCAGTGGACGAGCATTCTGGAGAAAGGC. Cre-mediated excision in myeloid cells from *Hdac7*$^{fl/fl}$/*LysM*^{Cre} mice was confirmed using the above F primer and R-GAGAGCCAGCTGCAGCGAGAAGTG.

Primary cell cultures

Mouse macrophages were cultured in RPMI-1640 or DMEM (Thermo Fisher Scientific) supplemented with 10% FCS, 20 U/mL penicillin, 20 U/mL streptomycin and 2 mM L-glutamine. BMM were derived from 6-10 week old mice in the presence of recombinant human colony-stimulating factor (CSF) 1 (1×10^4 U/ml) for 6 days. On day 6, cells were plated at the required density and treated the following day. $CD14^+$ human monocytes, which were purified from buffy coats provided by the Australian Red Cross Blood Service, were differentiated into HMDM by culturing for 7 days in recombinant human CSF-1 (1×10^4 U/mL) in supplemented IMDM as for mouse macrophages. We had no information on donor identity, and we presume that there were equal or similar numbers of male and female donors.

Cell lines

THP-1 cells were cultured in RPMI containing 1% HEPES (Thermo Fischer Scientific) and 1% sodium pyruvate, in addition to 10% FCS, 20 U/mL penicillin, 20 U/mL streptomycin and 2 mM L-glutamine. RAW 264.7 cells were cultured in RPMI containing 5% FCS, 20 U/mL penicillin, 20 U/mL streptomycin and 2 mM L-glutamine. HEK293T and PlatE cells were cultured in DMEM, supplemented with 10% FCS, 20 U/mL penicillin, 20 U/mL streptomycin. All cells were cultured at 37°C (unless otherwise indicated) and 5% CO_2.

Ethics statement

All studies involving animals were reviewed and approved by the appropriate University of Queensland animal ethics committee. Human peripheral blood was collected from healthy donors following informed consent, under approval by the University of Queensland Institutional Human Research Ethics Committee.

METHOD DETAILS

Preparation of HDAC inhibitors

The selective class IIa HDAC inhibitors TMP269 and TMP195 containing the trifluoromethyloxadiazole fragment were synthesized in house using the methods reported by Lobera et al. (2013) and described in the supporting information section. The material was characterized by ^1H and ^{13}C NMR spectroscopy, HRMS and all data was consistent with literature values. Purity determined by HPLC was > 98%. TMP269 and TMP195 were used at different concentrations in cell culture experiments as indicated. SAHA and MS-275 were also synthesized in-house, dissolved in DMSO at 10 mM, and diluted in tissue culture medium for cell culture treatments.

Generation of Hdac7 mutant (Hdac7ΔH649A) and molecular modeling

The Hdac7ΔH649A point mutant was created by site directed mutagenesis using a three-way PCR strategy. The mutation was confirmed by sequencing, and expression and function of the mutant was confirmed by transfecting in HEK293T cells followed by immunoblotting and class IIa HDAC enzyme assay, as described below. The crystal structure (pdb: 3C10) of the catalytic domain of human HDAC7 in complex with TSA was retrieved from the rcsb protein databank (http://www.rcsb.org/). Pymol (Molecular Graphics System, Version 1.6.0.0. Schrödinger, LLC) was used to visualize the protein-ligand complex structure and to create the modeling figure. The His672 (red) and Asn714 residues (corresponding to mouse His649 and Asn691) are shown in stick form, and the zinc atom is shown as a gray ball.

Generation of Pkm2 point mutants (K89R, K305R, K433R)

K-to-R point mutants in Pkm2 for the indicated lysine residues were created by site directed mutagenesis using a three-way PCR strategy. The mutations were confirmed by sequencing, and expression of the mutants were confirmed by transfecting in HEK293T cells followed by immunoblotting.

Retroviral transduction

2×10^6 PlatE packaging cells (Morita et al., 2000) were transfected with 40 μg of the indicated retroviral expression constructs using Lipofectamine 2000, after which cells were incubated overnight at 37°C. At 24 h post-transfection, media was changed and cells were incubated at 32°C overnight for optimal virus production. Viral supernatants were filtered using 0.45 μM Millex-HV PVDF syringe filters (Merck), and 1 M HEPES, 10 μg/ml polybrene and 1×10^4 U/ml CSF-1 were added. Day 2 CSF-1-induced BMM progenitors in 6-well plates were spin-infected (1000 *g*, 2 h, 35°C) with viral supernatants. The wells were supplemented with complete media, and then incubated at 37°C for 48 h. Media was again replaced with fresh CSF-1-containing media, and on the following day (day 4 of BMM differentiation), adherent cells were collected and plated for experiments on day 6.

Gene silencing

THP-1 cells were differentiated for 48 h with 30 ng/ml PMA. Cells (differentiated THP-1, HMDM or BMM) were inucubated at 2.5×10^6 cells/cuvette in 350 μL complete media containing 10 mM HEPES and the specific siRNA at 1 μM for human macrophages or 0.25 μM for BMM. The cells were electroporated at 260 V, 1000 μF and ∞ Ω (Bio-Rad), rested for 5 min, washed and plated. After 24 h, the media was changed and cells were primed with LPS for 4 h followed by treatment with nigericin (3 h for HMDM and THP-1, 30 min for BMM), treated with LPS alone for 4 h, or were left untreated. Supernatants were analyzed for secreted levels of indicated cytokines by

ELISA. MTT assays were performed in parallel to account for any difference in plating densities, with secreted levels of cytokines being normalized to MTT data. qPCR was performed to assess the degree of gene knockdown.

Cytokine analysis

BMM (2×10^5 cells/ml) were treated with LPS (100 ng/ml or as otherwise stated) and/or different inhibitors (3 to 30 μM TMP269; 0.5 to 2 μM TMP195, 10 μM HIF1α inhibitor, 5 mM 2-DG or 10 μM DASA) for the indicated time intervals. Supernatants were collected and analyzed for levels of different cytokines using commercially available ELISA kits. To assess secreted Il-1β by ELISA, cells were primed with LPS for the indicated time period, before treatment with nigericin (5 μg/ml) for 30 min to 1 h (BMM) or 3 h (HMDM and THP-1). For experiments comparing macrophages derived from mice of different genotypes, MTT assays were performed, with levels of secreted cytokines being normalized to MTT data in order to correct for any differences in the plating density.

Estimation of nitric oxide

BMM (2×10^5 cells/ml) were primed with Ifnγ (5 ng/ml) for 18 h, after which cells were treated with LPS (0.5 ng/ml or 100 ng/ml) for 24 h. Supernatants were collected and analyzed for levels of nitric oxide using Griess reagent (Promega).

Protein lysates and immunoblotting

Whole cell lysates were prepared in RIPA buffer. Nuclear and cytoplasmic fractions from 1×10^7 cells were separated by washing treated cells twice in ice cold PBS, then resuspending in hypotonic wash buffer (10 mM HEPES, pH 7.4, 1.5 mM $MgCl_2$ and 10 mM KCl containing Protease Inhibitor Cocktail (Roche), 1 mM PMSF, 1 mM sodium vanadate and PhosSTOP phosphatase inhibitors (Sigma)). Cells were incubated for 5 min on ice to swell cells, after which 0.1% NP-40 was added and incubated at room temperature for approximately 5 min to lyse cells. Nuclei were pelleted by centrifugation at 500 *g* for 5 min at 4°C and supernatants were collected as cytoplasmic fractions. Nuclei were washed three times in hypotonic wash buffer containing 0.1% NP-40, then lysed in nuclear extract buffer (20 mM HEPES, pH 7.8, 0.42 M NaCl, 20% glycerol, 0.2 mM EDTA, 1.5 mM $MgCl_2$ with Protease Inhibitor Cocktail, 1 mM PMSF, 1 mM sodium vanadate and PhosSTOP phosphatase inhibitors). Immunoblotting was performed on equal amounts of total protein (quantified using BCA assay, Pierce) using the indicated antibodies.

Size exclusion chromatography

1-2 × 10^6 BMM were pre-treated with DMSO or TMP269 for 1 h, then treated with LPS (100 ng/mL) for 24 h. Cells were washed in cold PBS and lysed in 50 mM Tris (pH 7.4), 150 mM NaCl, 1 mM EDTA, 1% Triton X-100, 0.2% sodium deoxycholate with 1 mM PMSF, Protease Inhibitor Cocktail and PhosStop phosphatase inhibitors. Lysates were passed through a 27G needle and the insoluble fractions were pelleted at 17,000 *g* at 4°C for 15 min. Cleared lysates were passed through a Superdex 200 10/300 GL column. Input lysates and resulting fractions were analyzed by immunoblotting for PKM2.

Co-immunoprecipitation

HEK293T cells were transiently transfected with the indicated constructs using Lipofectamine 2000 reagent. For experiments involving inhibitors, transfected cells were treated with the appropriate inhibitors, 8 h post-transfection. Whole cell lysates were prepared in RIPA buffer, 24 h post-transfection. V5-tagged proteins were immunoprecipitated and bound fractions were then immunoblotted for FLAG-tagged Pkm2.

Gene expression analyses

Cells were lysed in TRIzol (Invitrogen) and total RNA was extracted using RNA purification kits (Zymo Research), as per the manufacturer's instructions. DNase (Invitrogen) treated RNA were reverse transcribed to cDNA using Superscript III (Invitrogen) and oligo dT. Levels of specific mRNAs were quantified by qPCR using SyBR Green-PCR mix (Invitrogen) in the Applied Biosystems 7900HT fast RT-PCR system. Appropriate negative controls with no Superscript were included for all experiments. Results were expressed relative to the housekeeping gene, *Hprt* (mouse) or *HPRT* (human) using the ΔCt method (Livak and Schmittgen, 2001).

Proximity ligation assay/immunofluorescence

5x10^4 Mac-Hdac7 or MacBlue BMM on coverslips were fixed using 4% paraformaldehyde, washed in PBS then permeabilised and blocked using 0.1% Triton X-100 and 0.5% bovine serum albumin in PBS. Primary antibodies detecting V5 and Pkm2 or V5 and MAPK p38 were used in combination with Duolink *In Situ* Detection Reagents Orange, DAPI (Sigma) and wheat-germ agglutinin-Alexa Fluor 647 (Invitrogen, W32466) to detect PLA signal, DNA and cell boundary respectively. Coverslips were mounted on slides using Dako mounting media and cells were imaged at 63X using oil immersion with Carl Zeiss Meta Inverted LSM 510 microscope (Carl Zeiss) and processed using ImageJ. Cells (defined by wheat-germ agglutinin staining) with > 2 puncta were considered as PLA-positive cells, and quantification was performed in an unbiased fashion using the find maxima function in ImageJ (3-10 images analyzed in each experiment). Immunofluorescence was performed on BMM (5x10^4) retrovirally-transduced with empty vector, FLAG-tagged Pkm2 or Pkm2 K433R constructs. Coverslips were fixed using 4% paraformaldehyde, washed in PBS and blocked in blocking buffer (5% FCS, 0.3% Triton X-100 in PBS). Incubation in primary antibody was performed overnight using rabbit anti-FLAG (1 in 500 dilution in blocking buffer), followed by incubation with secondary antibody (anti-rabbit-Alexa Fluor 647, 1 in

400 dilution), DAPI and Phalloidin-Alexa Fluor 594 (Life Technologies, A12381) for 1 h. Coverslips were mounted on slides, sealed and imaged at 63X using oil immersion with a Carl Zeiss Meta Inverted LSM 510 microscope (Carl Zeiss).

Measurement of pyruvate kinase (PK) activity

BMM were cultured in DMEM under different conditions as stated. HEK293T cells were transiently transfected with the indicated constructs. Lysates were prepared at 24 h post-transfection. PK activity was measured by a PK assay kit, according to the manufacturer's instructions.

Metabolic flux analysis

100,000 BMM of the indicated genotypes were seeded in XF96 cell culture plates (Agilent) and either treated ± LPS (0.5 ng/ml or 100 ng/ml) in the presence or absence of TMP195 (2 μM) for 24 h. ECARs and OCRs were measured using XFe-96 Flux Analyzer and the Seahorse Wave Software (Seahorse Bioscience, Agilent). Changes in ECAR were measured by sequential injection of glucose (10 mM), oligomycin (1.5 μM) and 2-DG (50 mM). To measure changes in OCR, treated/untreated BMMs were injected sequentially with oligomycin (1.5 μM), FCCP (1 μM) and Rotenone/Antimycin A (0.5 μM), as indicated in Figure S2G. Three readings were taken before and after every injection. ECAR and OCR values were further used to quantify glycolytic and mitochondrial respiration parameters, respectively.

Glucose uptake by 2-NBDG

BMM were cultured in complete RPMI in the presence or absence of LPS (100 ng/ml or 0.5 ng/ml) and TMP195 (2 μM) for 24 h. Cells were washed once with phenol red-free DMEM supplemented with 10% FCS and 2 mM L-glutamine, before incubating with the media containing 2-NBDG (100 μM) for an hour. The cells were washed twice with PBS to remove any residual 2-NBDG before analyzing the amount of 2-NBDG uptake by flow cytometry.

Measurement of extracellular lactate

BMM were cultured in DMEM in the presence or absence of LPS and the indicated inhibitors. Lactate levels in the culture medium were determined using a colorimetric L-Lactate Assay Kit, according to the manufacturer's instructions.

Class IIa HDAC enzyme assay

HEK293T cells were transfected with pEF6-V5-based mammalian expression plasmids for wild-type Hdac7, enzyme-dead Hdac7 (H649A) or an unrelated protein (Sox7). At 24 h post-transfection, cells were lysed using a mild lysis buffer (50 mM Tris HCl, 150 mM NaCl, 1 mM EDTA, 1% NP40), without protease inhibitors. For HDAC activity assays, the cell lysates were diluted appropriately in HDAC assay buffer (50 mM Tris HCl, 137 mM NaCl, 2.7 mM KCl, 1 mM $MgCl_2$, pH 8.0) and incubated ± the indicated HDAC inhibitor for 30 min. The class IIa-specific HDAC substrate (Ac-Leu-Gly-Lys(TFAc)-AMC) (Lobera et al., 2013) (200 μM) was added to samples, after which they were incubated at 37°C for 30 min. Reactions were quenched using a stop solution containing 20 mM SAHA and 1 mg/ml Trypsin (Sigma). Fluorescence was measured at 460 nm using a FLUOstar OPTIMA microplate reader (BMG LABTECH) and the MARS Data Analysis Software (BMG LABTECH). HEK293T lysates were also immunoblotted to account for levels of ectopic protein expression, to normalize enzyme activity. For inhibitor screening, equal volumes of lysates were treated with DMSO or TMP269 for 15 min prior to addition of the class IIa-specific HDAC substrate.

Rapid immunoprecipitation mass spectrometry of endogenous proteins (RIME)

A detailed protocol for RIME has been described (Mohammed et al., 2016). In brief, 3×10^7 BMM were cross-linked with 1% formaldehyde (Thermo Fisher Scientific) at room temperature for 8 min, the reaction was quenched with 0.1 M Glycine (pH 7.5) and cells were washed twice with cold PBS. Cells were harvested in cold PBS containing protease inhibitors, lysed sequentially with LB1 (50 mM HEPES-KOH pH 7.5, 140 mM NaCl, 1 mM EDTA, 10% Glycerol, 0.5% NP-40, 0.25% Triton X-100), LB2 (10 mM Tris-HCl pH 8.0, 200 mM NaCl, 1 mM EDTA, 0.5 mM EGTA), and then LB3 (10 mM Tris-HCl pH 8.0, 100 mM NaCl, 1 mM EDTA, 0.5 mM EGTA, 0.1% sodium deoxycholate, 0.5% N-lauroylsarcosine) all containing protease inhibitors and sonicated using a 30 s on/30 s off cycle for 10 min. 1% Triton X-100 was added to the lysate and centrifuged at 20,000 *g* for 10 min at 4°C. Supernatants were transferred to fresh tubes and Protein G magnetic beads (Thermo Fisher Scientific) bound to anti-V5 were incubated with lysate overnight at 4°C on a rotator. Beads were washed 6 times in RIPA buffer with protease inhibitors, followed by two washes in freshly made 100 mM ammonium hydrogen carbonate. In-solution digests were performed on the washed beads using 10 ng/μL sequencing grade Trypsin (Promega). Following overnight digestion, peptides were dried by vacuum centrifugation, reconstituted in 0.1% formic acid and analyzed by LC-MS/MS on a Shimadzu Prominence Nano HPLC (Japan) coupled to a Triple TOF 5600 mass spectrometer (ABSCIEX). Protein identification was performed using ProteinPilot v4.5 against the UniProt_Sprot_20130205 database. Search parameters were defined as a thorough search using trypsin digestion and all entries in the database. Proteins were considered as a specific Hdac7-binding partner if there was at least one peptide identified with 99% confidence, and they were not present in anti-V5 pull downs from macrophage extracts from either the MacBlue or UAS-Hdac7 controls. The top 8 proteins listed in Figure 2A were

detected only in Mac-Hdac7 macrophages and with 2 or more peptides at ≥ 95% confidence. The ms score denotes the measurement of peptide confidence from the ProteinPilot scoring algorithm, Score = -log(1-(PercentConfidence/100)). For example, a score of 5 = 99.9% confidence.

Mass spectrometric identification of acetylated lysine residues

HEK293T cells were transiently transfected with FLAG-Pkm2 constructs using Lipofectamine L2000. At 24 h post-transfection, the cells were treated with TMP269 (30 μM) for an additional 24 h. Whole cell lysates were prepared in RIPA buffer and FLAG-tagged proteins were immunoprecipitated. Immunoprecipitated proteins were separated using 4%–12% SDS-PAGE and stained using Coomassie brilliant blue. Appropriate sized bands were excised and in-gel digestion was performed using sequencing grade Trypsin/Lys-C mix (Promega), overnight. Digested peptides were dried by vacuum centrifugation and reconstituted in 0.1% formic acid. Peptides were separated and detected by LC-MS/MS on a Shimadzu Prominence Nano HPLC (Japan) coupled to a Triple TOF 5600 mass spectrometer (ABSCIEX). Identified peptides were analyzed using ProteinPilot v5 against Uniprot database for mouse Pkm2. Search parameters were restricted to a thorough search for acetylation sites in the database. The intensities of target peptides (GDLGIEI PAEKV for K305 and SGAIIVLTK for K433) in control versus TMP269-treated samples were normalized to that of a non-acetylated highly abundant peptide (KGSGTAEVELK) from the same samples. This was then used to calculate the fold increase in hyperacetylation of the particular lysine residues in TMP269-treated samples.

Metabolic profiling of LPS-activated macrophages

1×10^7 BMM were treated with DMSO, LPS (100 ng/mL) + DMSO or LPS + TMP269 (30 μM) for 24 h. Cells were washed in cold PBS, then polar metabolites were extracted using a modified Bligh-Dyer water/methanol/chloroform extraction procedure at a 1/2/3 ratio, as previously described (McDonald et al., 2014). Central carbon metabolites were measured using liquid chromatography tandem mass spectrometry analysis. Liquid chromatography tandem mass spectrometry data were acquired on a Dionex UltiMate 3000 liquid chromatography system (Dionex) coupled to an ABSciex 4000 QTRAP mass spectrometer (ABSciex), and processed in MultiQuant 2.1 software (ABSciex), as previously described (Medina-Torres et al., 2015).

Cell-free protein expression using the Leishmania tarentolae system and protein-protein interaction studies by AlphaLISA assays

N-terminal Hdac7 (23-504), C-terminal Hdac7 (498-938) and full length PKM2 were sub-cloned into Gateway cloning compatible *Leishmania* expression vectors with fusions of N-terminal- GFP and C-terminal-mCherry (Gagoski et al., 2015). The *Leishmania tarentolae* extract and the feeding solution for protein expression were prepared as previously described (Johnston and Alexandrov, 2014). Each N-term and C-term truncated form of Hdac7 (labeled with C-terminal mCherry) was co-translated with N-terminally eGFP-tagged Pkm2 in the *Leishmania tarentolae* extract expression system. The AlphaLISA acceptor and donor beads (Perkin Elmer) were diluted in Universal assay buffer (Perkin Elmer) according to the manufacturer's protocol (PerkinElmer, 2016). The cell-free co-expressed proteins were incubated with the acceptor beads for 1 h at room temperature, followed by addition of donor beads. The samples were incubated for 30 min at room temperature under subdued light and incubated. The AlphaLISA signal was detected with a microplate reader (Tecan). As a negative control for the assay, the FKBP-rapamycin-binding domain of mTOR (as a non-interacting partner of Pkm2) was co-translated with Pkm2.

Cell death quantification

BMM were primed with LPS for 4 h in the presence or absence of TMP269. Cells were then treated with nigericin (5 μg/ml) for 30 min to induce pyroptosis. Lactate dehydrogenase (LDH) released into the culture supernatants, was measured using the LDH activity assay kit, as per the manufacturer's instructions.

LPS-induced inflammation model

For experiments in transgenic Mac-Hdac7 mice or littermate control genotypes, mice housed under specific-pathogen free conditions, were injected intra-peritoneally with 2 mg/kg LPS in PBS or an equivalent volume of PBS (controls). For experiments with TMP195 in C57BL/6J mice, animals were administered equivalent volumes of either DMSO or 50 mg/kg TMP195 an hour prior to intra-peritoneal injection with either 2 mg/kg LPS or equivalent volume of PBS. Core body temperature using rectal thermometer was recorded at the indicated time points. Mice were euthanized at 4 h post-challenge, and blood was collected by cardiac puncture. Blood was allowed to clot overnight at 4°C. Samples were centrifuged at 2000 *g* for 10 min, and the serum layer was collected and stored at −80°C until analysis. Levels of serum cytokines were quantified using the Legendplex Mouse Inflammation Panel, as per the manufacturer's instructions. Data was collected on a BD FACSCanto II cytometer and analyzed using the Legendplex data analysis software provided. Il-12p40 and Il-1β ELISA were performed separately using matched antibody pairs as described.

QUANTIFICATION AND STATISTICAL ANALYSIS

Each experiment was performed with at least two technical duplicate samples. For each experiment, the average of these technical replicates was used when combining data from independent experiments. Statistical analyses were performed on data combined

from 3 or more independent experiments, using Prism 7 software (Graph-Pad) with error bars indicating the standard error of the mean (SEM). For datasets with 3 or more variables, a one-way or two-way analysis of variance (ANOVA) was performed followed by Tukey's or Sidak's multiple comparison test. For data with two variables, unpaired t tests were performed. Differences with confidence values of 95% ($p < 0.05$) were considered to be statistically significant.

DATA AND CODE AVAILABILITY

This study did not generate any unique datasets or code.

Cell Reports, Volume *30*

Supplemental Information

Class IIa Histone Deacetylases Drive Toll-like Receptor-Inducible Glycolysis and Macrophage Inflammatory Responses via Pyruvate Kinase M2

Kaustav Das Gupta, Melanie R. Shakespear, James E.B. Curson, Ambika M.V. Murthy, Abishek Iyer, Mark P. Hodson, Divya Ramnath, Vikas A. Tillu, Jessica B. von Pein, Robert C. Reid, Kathryn Tunny, Daniel M. Hohenhaus, Shayli Varasteh Moradi, Gregory M. Kelly, Takumi Kobayashi, Jennifer H. Gunter, Alexander J. Stevenson, Weijun Xu, Lin Luo, Alun Jones, Wayne A. Johnston, Antje Blumenthal, Kirill Alexandrov, Brett M. Collins, Jennifer L. Stow, David P. Fairlie, and Matthew J. Sweet

A

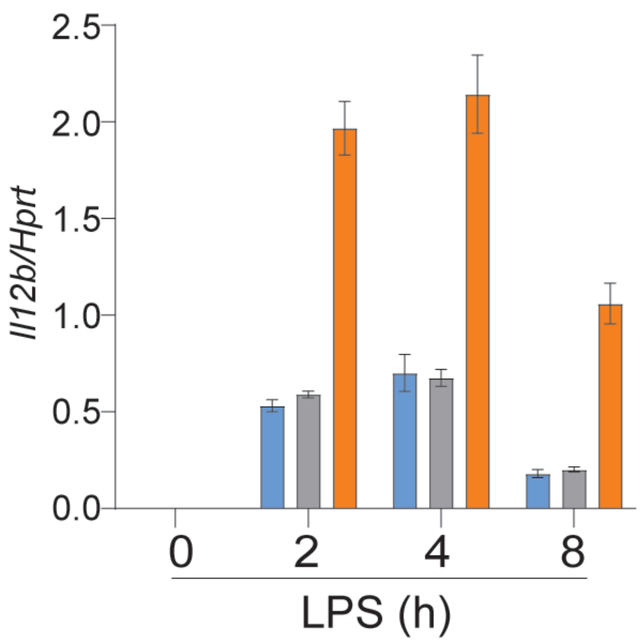

B

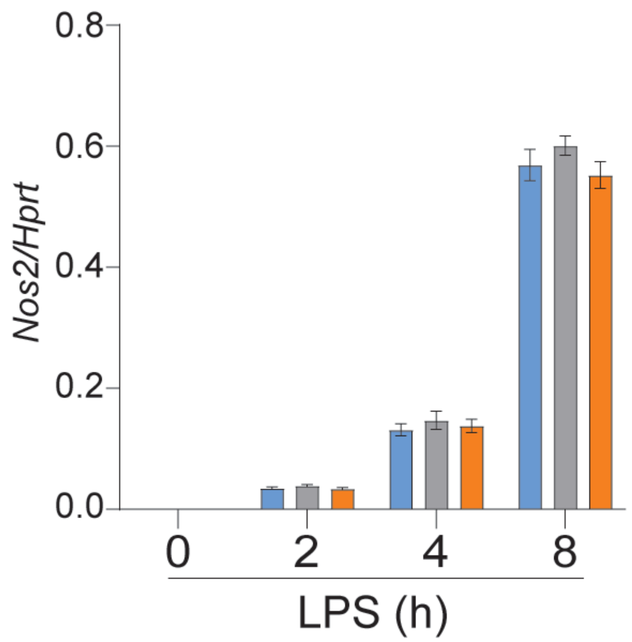

C

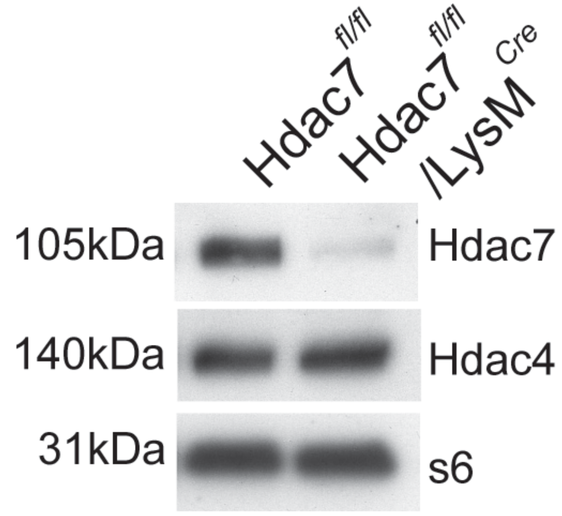

D

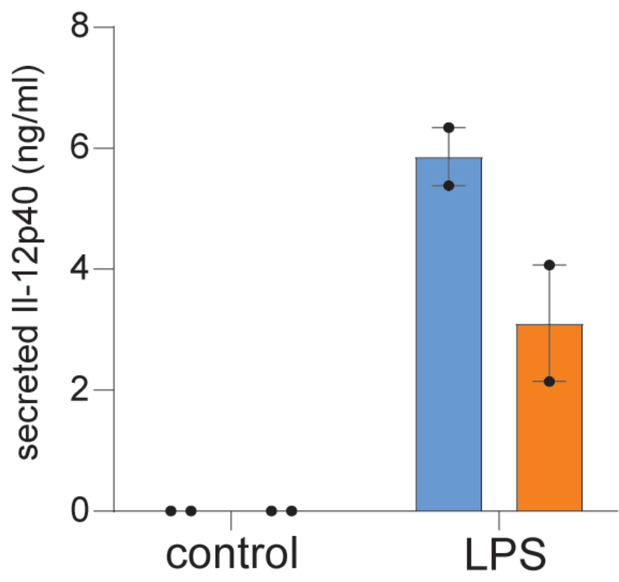

E

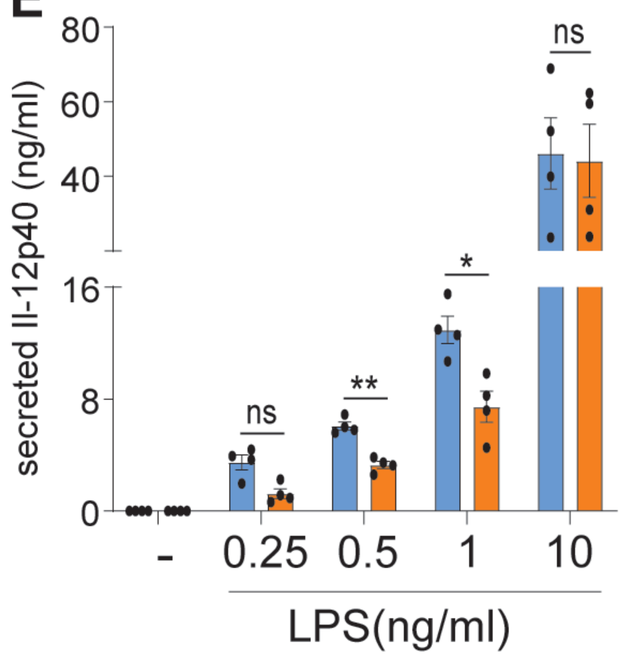

secreted Il-12p40 (ng/ml)

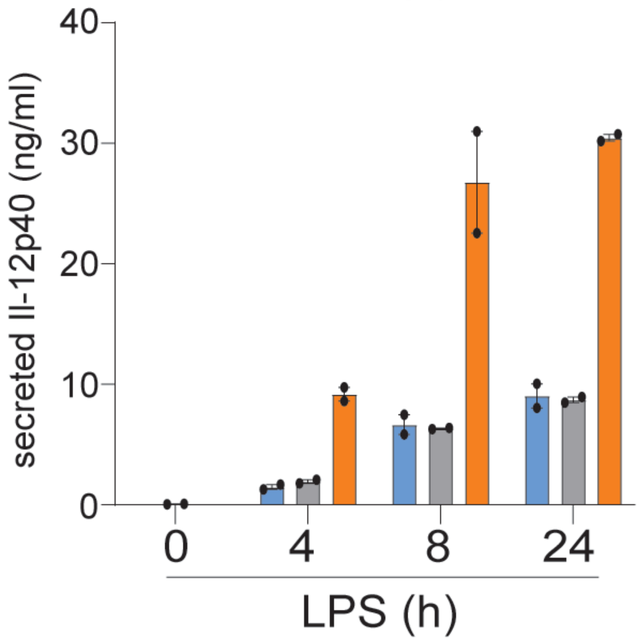

Nitrite (μM)

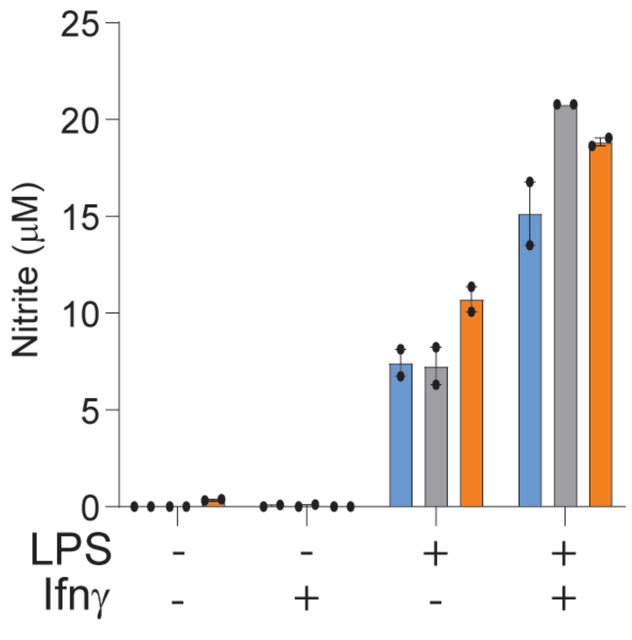

F

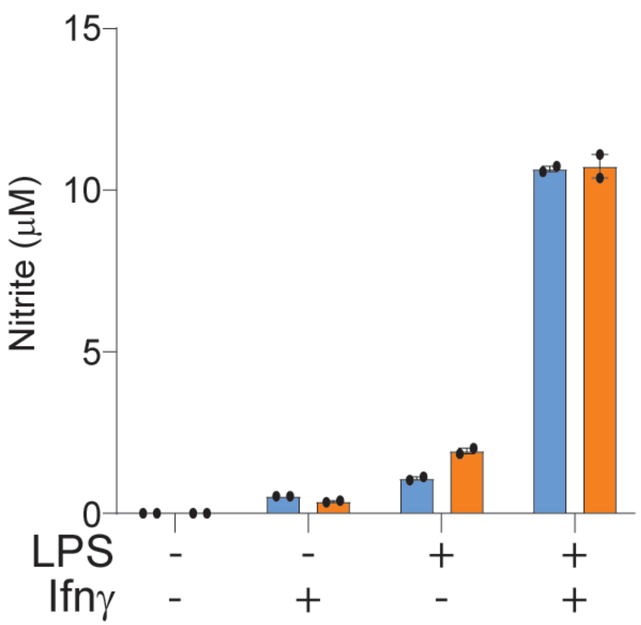

G

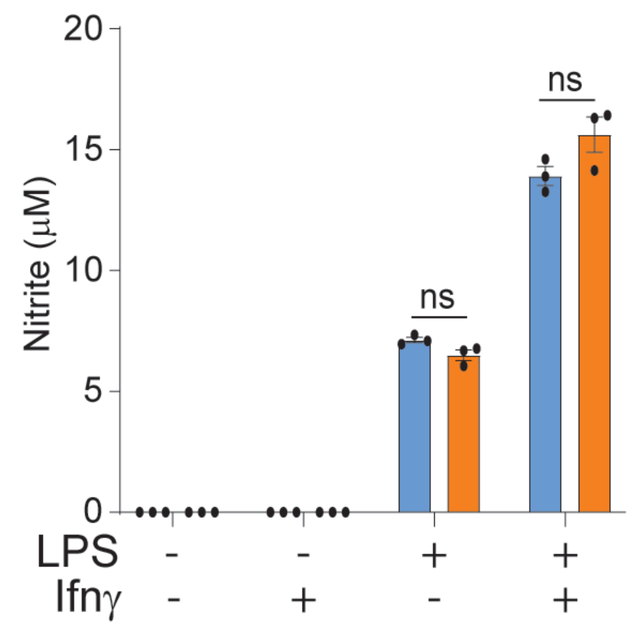

H

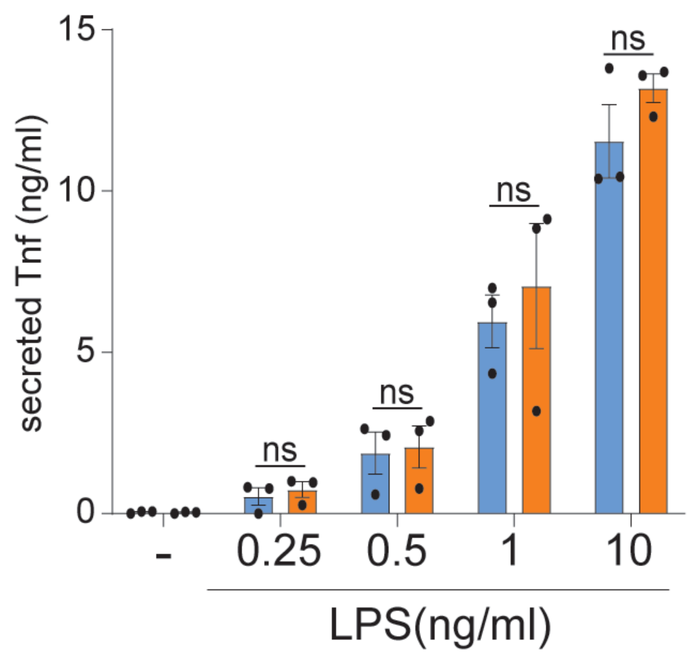

Supplementary Figure 1 – Related to Figure 1

(**A**) Indicated BMM populations were treated with LPS (100 ng/ml), and levels of *Il12b* mRNA (**top**) and secreted Il-12p40 (**bottom**) were quantified by qPCR and ELISA, respectively. Data are from a single experiment (representative of three experiments).

(**B**) Indicated BMM populations were treated with LPS (100 ng/ml) and mRNA levels of *Nos2* were determined by qPCR (**top**). Additionally, BMM were primed with Ifnγ (5 ng/ml) for 18 h, followed by treatment with LPS (100 ng/ml) for 24 h, after which NO production was assessed (**bottom**). Data are from a single experiment (representative of three experiments).

(**C**) Lysates from *Hdac7*$^{fl/fl}$/*LysM*^{Cre} and littermate control (*Hdac7*$^{fl/fl}$) BMM were immunoblotted for endogenous Hdac7 and Hdac4. The displayed immunoblot is representative of three independent experiments.

(**D**) Indicated BMM populations were stimulated with LPS (0.5 ng/ml) for 4 h. Levels of secreted Il-12p40 were determined by ELISA. Data are from a single experiment (representative of three experiments).

(**E**) Indicated BMM populations were stimulated across an LPS concentration range (0.25-10 ng/ml) for 4 h. Levels of secreted Il-12p40 were determined by ELISA.

(**F-G)** Indicate BMM populations were primed with Ifnγ (5 ng/ml) for 18 h, followed by treatment with LPS (0.5 ng/ml) (**F**) or (100 ng/ml) (**G**) for 24 h, after which NO production was assessed. Data in (**F**) are from a single experiment (representative of three experiments).

(**H**) Indicated BMM populations were stimulated across an LPS concentration range (0.25-10 ng/ml) for 4 h. Levels of secreted Tnf were determined by ELISA.

All graphical data are combined from three to four independent experiments, unless otherwise stated. Statistical significance was determined by two-way ANOVA, followed by Tukey's multiple comparison test (ns – not significant; * $p<0.05$; ** $p<0.01$).

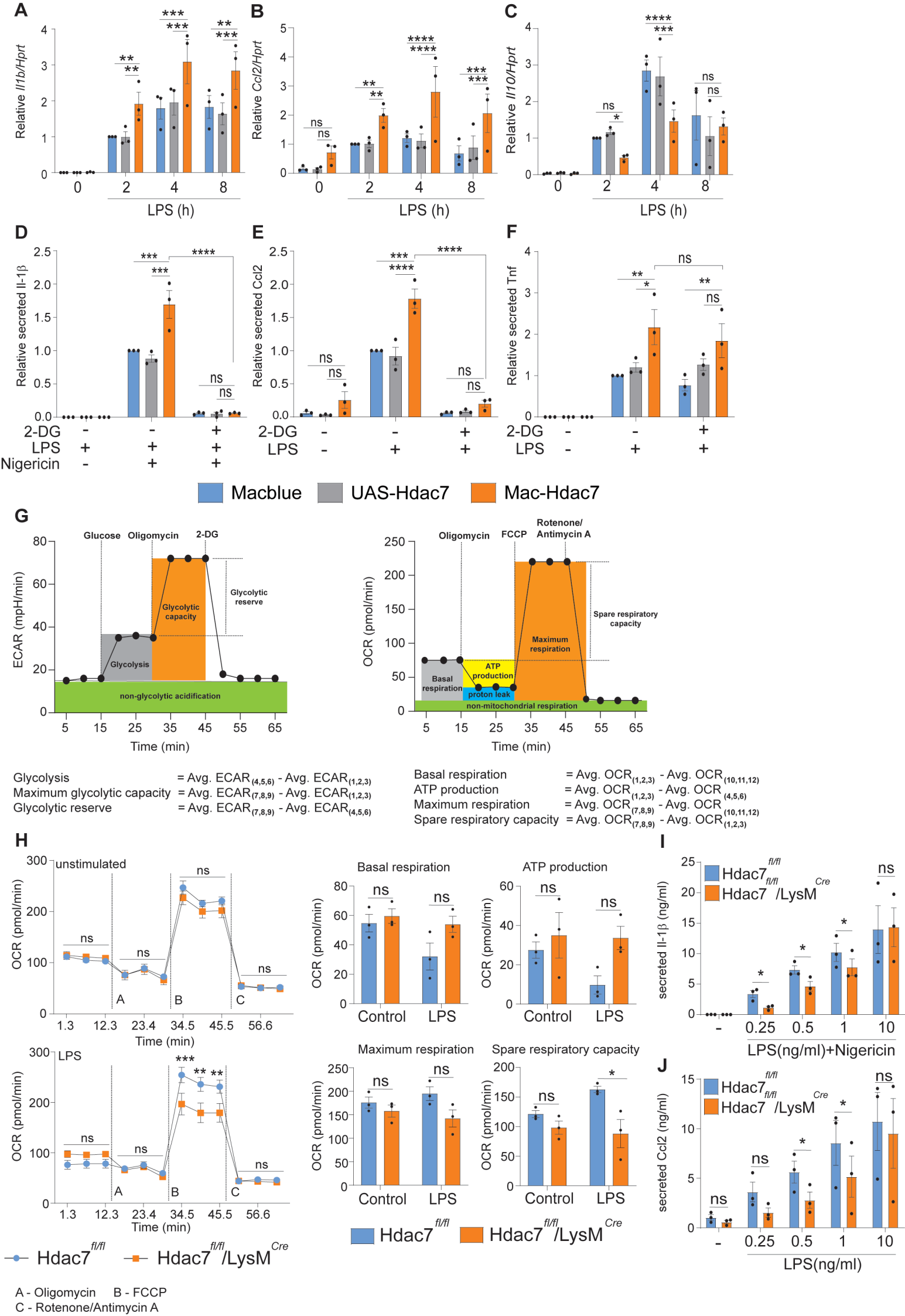

Glycolysis = Avg. ECAR$_{(4,5,6)}$ - Avg. ECAR$_{(1,2,3)}$
Maximum glycolytic capacity = Avg. ECAR$_{(7,8,9)}$ - Avg. ECAR$_{(1,2,3)}$
Glycolytic reserve = Avg. ECAR$_{(7,8,9)}$ - Avg. ECAR$_{(4,5,6)}$

Basal respiration = Avg. OCR$_{(1,2,3)}$ - Avg. OCR$_{(10,11,12)}$
ATP production = Avg. OCR$_{(1,2,3)}$ - Avg. OCR$_{(4,5,6)}$
Maximum respiration = Avg. OCR$_{(7,8,9)}$ - Avg. OCR$_{(10,11,12)}$
Spare respiratory capacity = Avg. OCR$_{(7,8,9)}$ - Avg. OCR$_{(1,2,3)}$

Supplementary Figure 2 – Related to Figure 3

(**A-C**) The indicated BMM populations were stimulated with LPS (100 ng/ml) for 2, 4 or 8 h, after which mRNA levels of *Il1b, Ccl2,* and *Il10* were determined by qPCR.

(**D-F**) The indicated BMM populations were pre-treated with 2-DG (5 mM) for 3 h, prior to treatment with LPS (100 ng/ml) for 4 h. Levels of nigericin-triggered Il-1β release (**D**), Ccl2 (**E**) and Tnf (**F**) were measured by ELISA.

(**G**) Schematic representation of calculations of glycolytic (**left**) and mitochondrial respiration (**right**) parameters from ECAR and OCR, respectively.

(**H**) The indicated BMM populations were either left untreated or treated with LPS (0.5 ng/ml, 24h). To measure OCR by Seahorse XFe96 analyser, cells were sequentially treated with Oligomycin, FCCP and Rotenone/Antimycin A. Cell counting by Hoechst was performed to normalize the data for any differences in plating density. Mitochondrial respiration-related parameters were calculated from measured OCR levels.

(**I-J**) The indicated BMM populations were stimulated across an LPS concentration range (0.25-10 ng/ml) for 4 h. Secreted levels of Il-1β (post-treatment with nigericin) (**I**) and Ccl2 (**J**) were determined by ELISA.

Data in **A-F** were normalized to Macblue control. Statistical significance was determined by two-way ANOVA, followed by Tukey's multiple comparison test (ns – not significant; * $p<0.05$; ** $p<0.01$; *** $p<0.001$; **** $p<0.0001$).

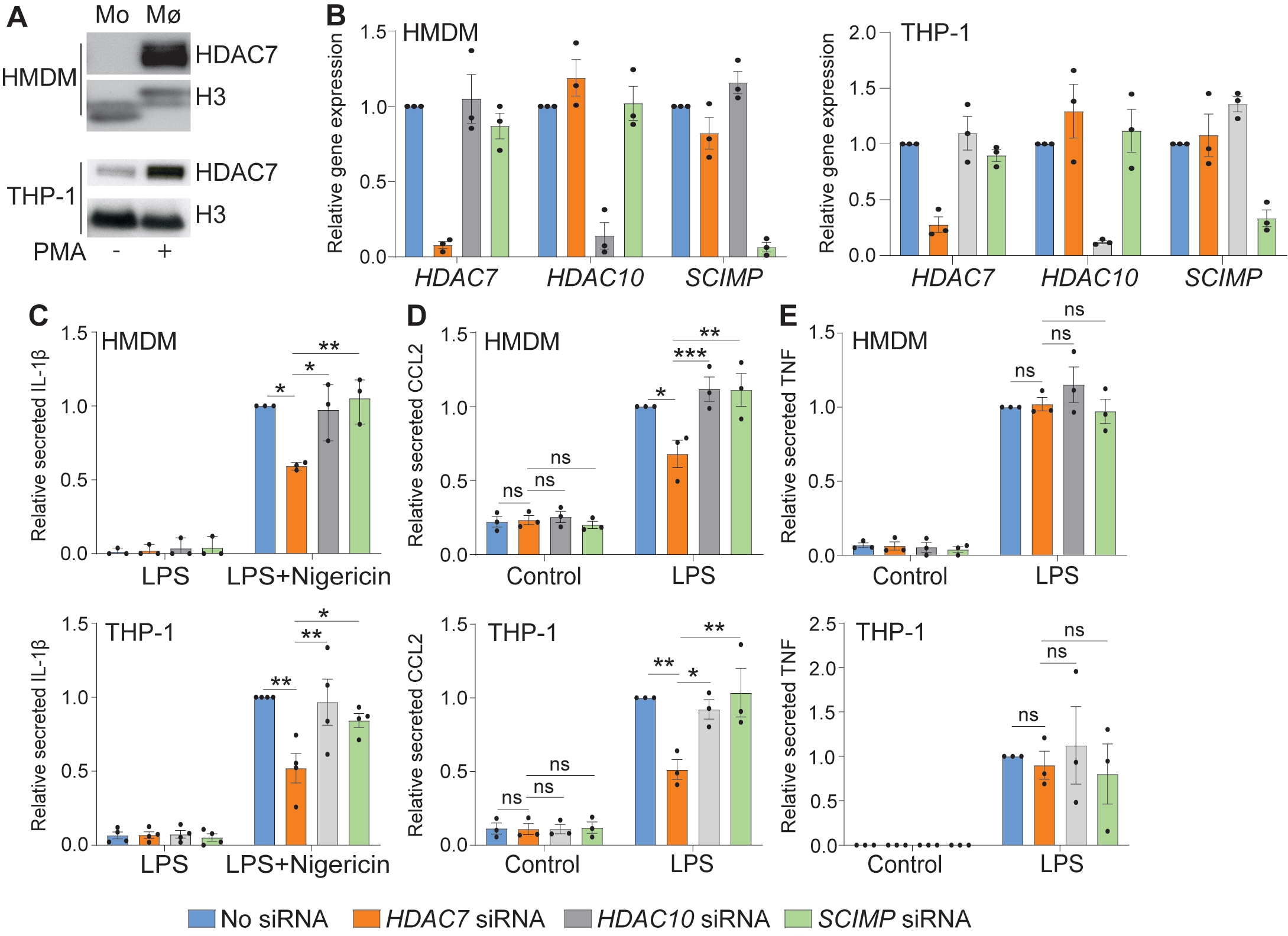
A
Mo
Mø
HMDM
HDAC7
H3
THP-1
HDAC7
H3
PMA
-
+
B
HMDM
Relative gene expression
HDAC7
HDAC10
SCIMP
THP-1
Relative gene expression
HDAC7
HDAC10
SCIMP
C
HMDM
Relative secreted IL-1β
LPS
LPS+Nigericin
THP-1
Relative secreted IL-1β
LPS
LPS+Nigericin
D
HMDM
Relative secreted CCL2
Control
LPS
THP-1
Relative secreted CCL2
Control
LPS
E
HMDM
Relative secreted TNF
Control
LPS
THP-1
Relative secreted TNF
Control
LPS
ns
No siRNA
HDAC7 siRNA
HDAC10 siRNA
SCIMP siRNA

Supplementary Figure 3 – Related to Figure 3

(A) Donor-matched human monocytes (Mo) and monocyte-derived macrophages (HMDM, Mϕ) (**top**) and THP-1 cells ± PMA (**bottom**) were analysed for HDAC7 levels by immunoblotting. Data are representative of four donors (monocytes/HMDM) or three experiments (THP-1).

(**B**) HMDM (**left**) and PMA-differentiated THP-1 (**right**) were transfected with the indicated siRNAs. Total RNA was collected from siRNA-transfected HMDM and THP-1, after which mRNA levels of *HDAC7*, *HDAC10* and an unrelated control gene, *SCIMP* were determined by qPCR.

(**C-E**) Transfected HMDM (**top**) or THP-1 (**bottom**) were stimulated with LPS (100 ng/ml) for 4 h. Levels of secreted IL-1β (post-treatment with nigericin) (**C**), CCL2 (**D**) and TNF (**E**) in culture supernatants were measured by ELISA.

Graphical data were normalized to the LPS-treated no siRNA control. Data in **B-E** (mean±SEM) are combined from three to four independent experiments. Statistical significance was determined by one-way ANOVA for **B** and two-way ANOVA for **C-E**, followed by Tukey's multiple comparison test (ns – not significant; * $p<0.05$; ** $p<0.01$; *** $p<0.001$).

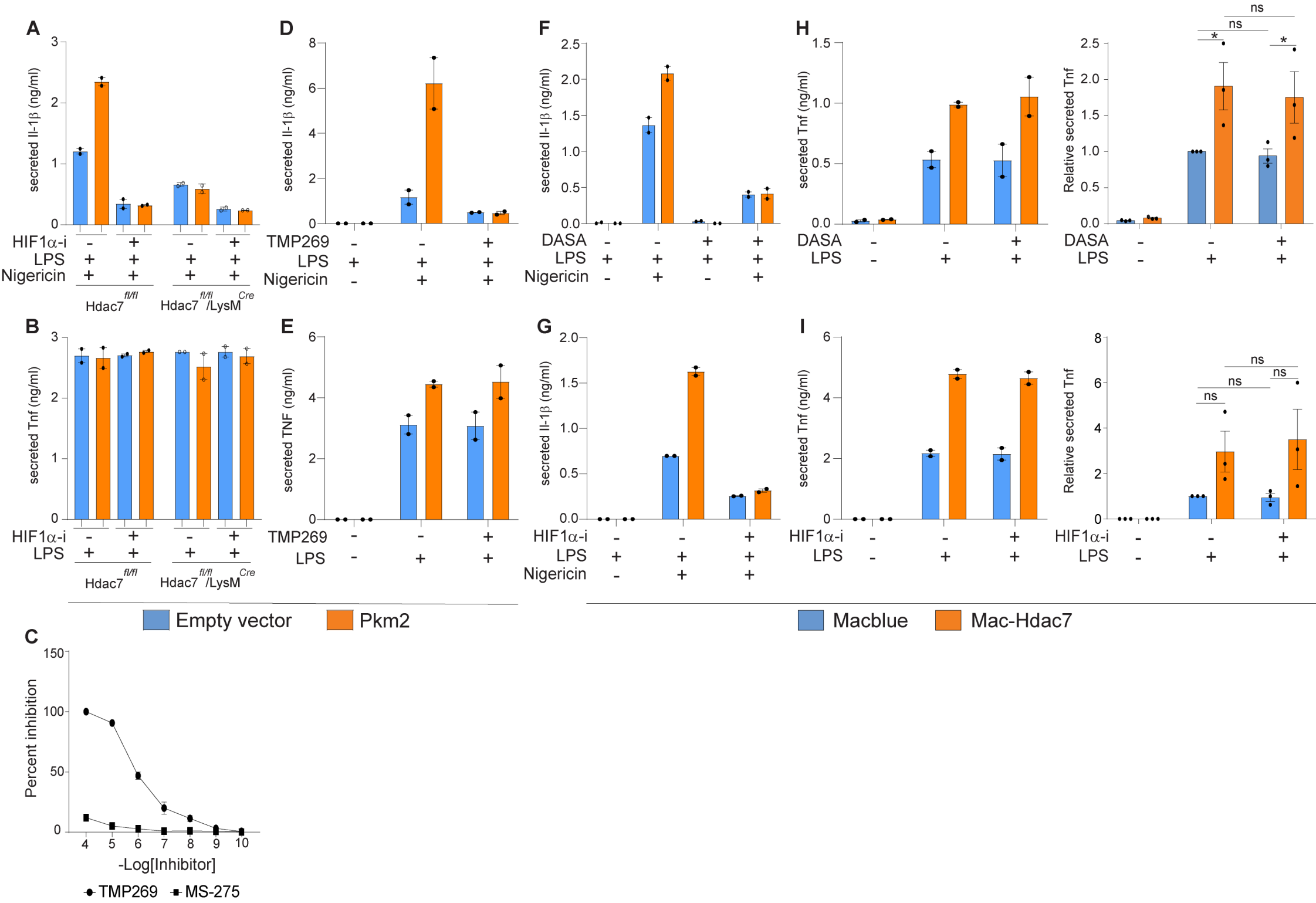
A
secreted Il-1β (ng/ml)
HIF1α-i
LPS
Nigericin
Hdac7fl/fl
Hdac7fl/fl/LysMCre
B
secreted Tnf (ng/ml)
HIF1α-i
LPS
Hdac7fl/fl
Hdac7fl/fl/LysMCre
C
Percent inhibition
-Log[Inhibitor]
TMP269
MS-275
D
secreted Il-1β (ng/ml)
TMP269
LPS
Nigericin
E
secreted TNF (ng/ml)
TMP269
LPS
F
secreted Il-1β (ng/ml)
DASA
LPS
Nigericin
G
secreted Il-1β (ng/ml)
HIF1α-i
LPS
Nigericin
H
secreted Tnf (ng/ml)
DASA
LPS
Relative secreted Tnf
ns
*
I
secreted Tnf (ng/ml)
HIF1α-i
LPS
Relative secreted Tnf
ns
Empty vector
Pkm2
Macblue
Mac-Hdac7

Supplementary Figure 4 – Related to Figure 4

(**A-B**) Indicated BMM populations were retrovirally-transduced with either empty vector or Pkm2 expression constructs, then treated with 0.5 ng/ml LPS for 4 h ± a HIF1α inhibitor (HIF1αi, 10 μM). Levels of nigericin-triggered Il-1β (**A**) and Tnf (**B**) were measured by ELISA. Data are from a single experiment (representative of three experiments).

(**C**) HEK293T cells were transiently transfected with an Hdac7 expression plasmid, and at 24 h post-transfection, a class IIa HDAC enzyme assay was performed on cellular lysates in the presence of different concentrations (10^{-4} M to 10^{-10} M) of the class IIa HDAC-selective inhibitor, TMP269 or the class I HDAC inhibitor, MS-275. Percentage inhibition of enzyme activity at different concentrations of the inhibitors was calculated relative to cell lysates incubated with vehicle only.

(**D-E**) BMM were retrovirally-transduced as above, then treated with 100 ng/ml LPS for 4 h in the presence or absence of TMP269 (30 μM). Levels of nigericin-triggered Il-1β (**D**) and Tnf (**E**) were measured by ELISA. Data are from a single experiment (representative of four experiments).

(**F-G**) The indicated BMM populations were treated with LPS (100 ng/ml) in the presence or absence of DASA (10 μM) for 4 h (**F**) or a HIF1αi (10 μM) (**G**) for 8 h, after which levels of nigericin-triggered Il-1β were measured by ELISA.

(**H-I**) The indicated BMM populations were treated with LPS (100 ng/ml) in the presence or absence of DASA (10 μM) for 4 h (**H**) or Hif1αi (10 μM) for 8 h (**I**). Levels of Tnf were measured by ELISA. Data from a single experiment are on the **left**, with combined data from three independent experiments on the **right**. Combined data in panel **H** and **I** (**right**) were normalized to the Macblue control. Statistical significance for **H** and **I** (panels on **right**) was determined by two-way ANOVA, followed by Tukey's multiple comparison test (ns – not significant; * $p<0.05$).

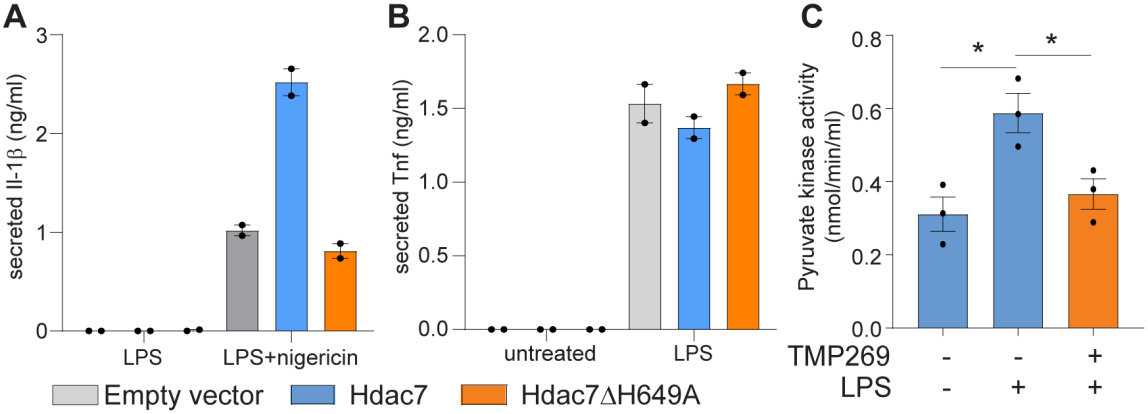

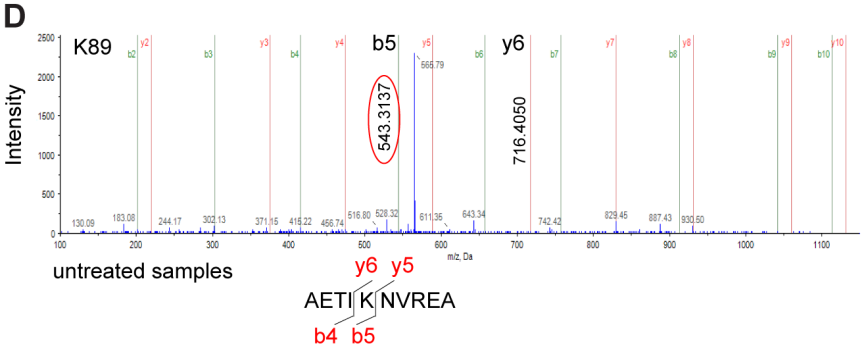

Residue	untreated b	TMP269 b
A	72.0444	72.0444
E	201.0870	201.0870
T	302.1347	302.1347
I	415.2187	415.2187
K(-Ac)	**543.3137**	**585.3243**
N	657.3566	699.3672
V	756.4250	798.4356
R	912.5261	954.5367
E	1041.5687	1083.5793
A	1112.6058	1154.6164
T	-	1255.6641

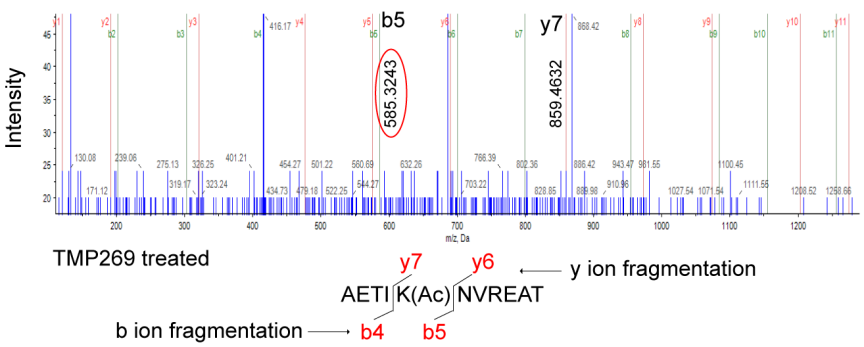

Residue	untreated y	TMP269 y
A	1130.6164	1273.6747
E	1059.5793	1202.6375
T	930.5367	1073.5949
I	829.4890	972.5473
K(-Ac)	**716.4050**	**859.4632**
N	588.3100	689.3577
V	474.2671	575.3148
R	375.1987	476.2463
E	219.0975	320.1452
A	90.0550	191.1026
T	-	120.0655

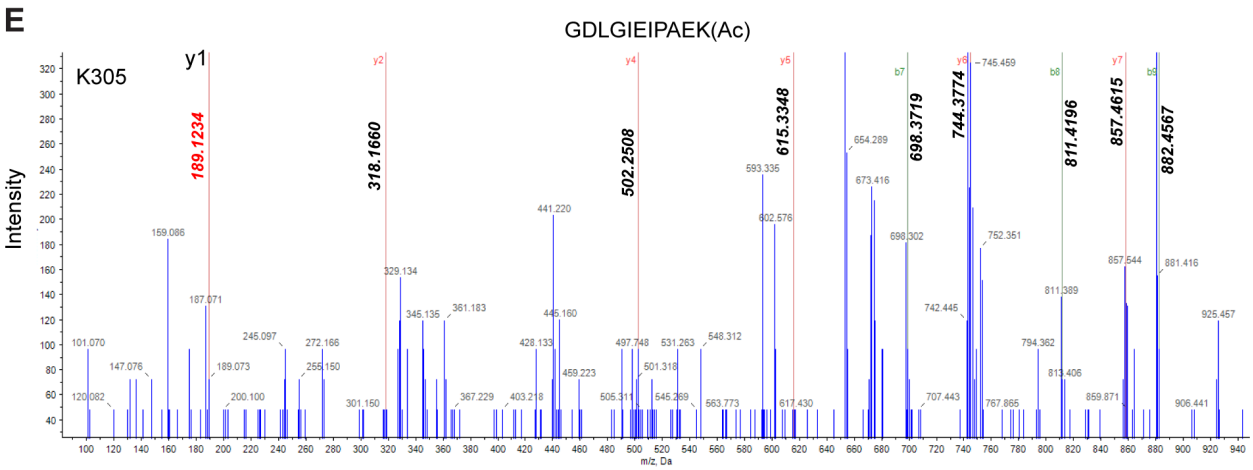

Residue	b	y
G	58.0287	1199.6154
D	173.0557	1142.5939
L	286.1397	1027.5670
G	343.1612	914.4829
I	456.2453	***857.4615***
E	585.2879	***744.3774***
I	***698.3719***	***615.3348***
P-Ox	***811.4196***	***502.2508***
A	***882.4567***	389.2031
E	1011.4993	***318.1660***
K-Ac	1181.6048	***189.1234***

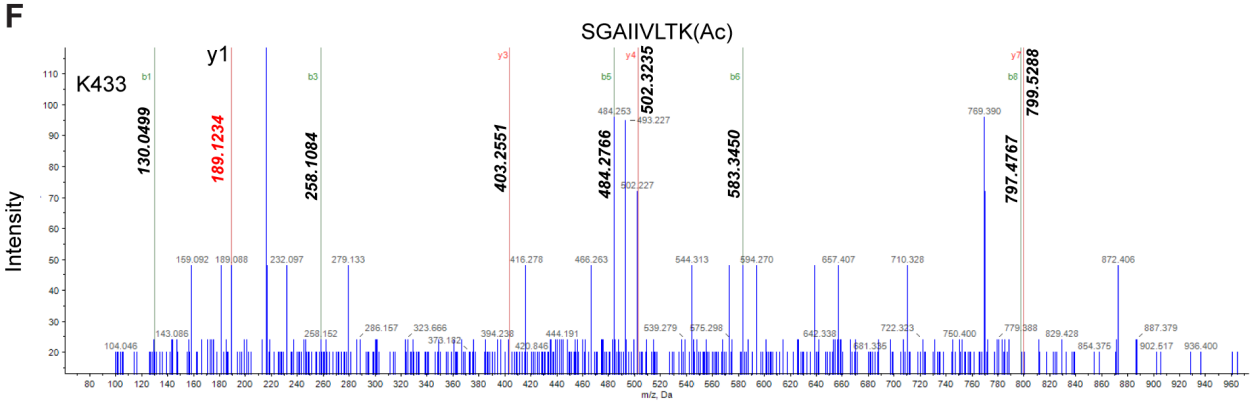

Residue	b	y
S	***130.0499***	985.5928
G	187.0713	856.5502
A	***258.1084***	***799.5288***
I	371.1925	728.4917
I	***484.2766***	615.4076
V	***583.3450***	***502.3235***
L	696.4291	***403.2551***
T	***797.4767***	290.1710
K-Ac	967.5823	***189.1234***

Supplementary Figure 5 – Related to Figure 5

(**A-B**) BMM from *Hdac7*$^{fl/fl}$/*LysM*^{Cre} mice were retrovirally-transduced with the indicated constructs, then treated with 0.5 ng/ml LPS for 4 h. Levels of nigericin-triggered Il-1β (**A**) and Tnf (**B**) were measured by ELISA. Data are from a single experiment (representative of three experiments).

(**C**) PK assays were performed on lysates from the BMM populations treated ± LPS (0.5 ng/ml) for 4 h in the presence or absence of TMP269 (30 μM).

(**D-F**) HEK293T cells were transfected with Pkm2-FLAG constructs. At 24 h post-transfection, cells were treated with TMP269 (30 μM) and cell lysates were collected at 48 h post-transfection. FLAG-Pkm2 was purified by IP with anti-FLAG antibody and subjected to SDS-PAGE. The Coomassie-stained band for Pkm2 was digested and subjected to mass spectrometric analysis using Triple TOF 5600 mass spectrometer. The peptide list generated was analysed using Protein Pilot. Spectra displayed here indicates the acetylation status of lysine residues K89 (**D**), K305 (**E**) and K433 (**F**) in control and TMP269-treated cells (**D**) or TMP269-treated cells (**E-F**), as assessed by the b and y ion fragmentation.

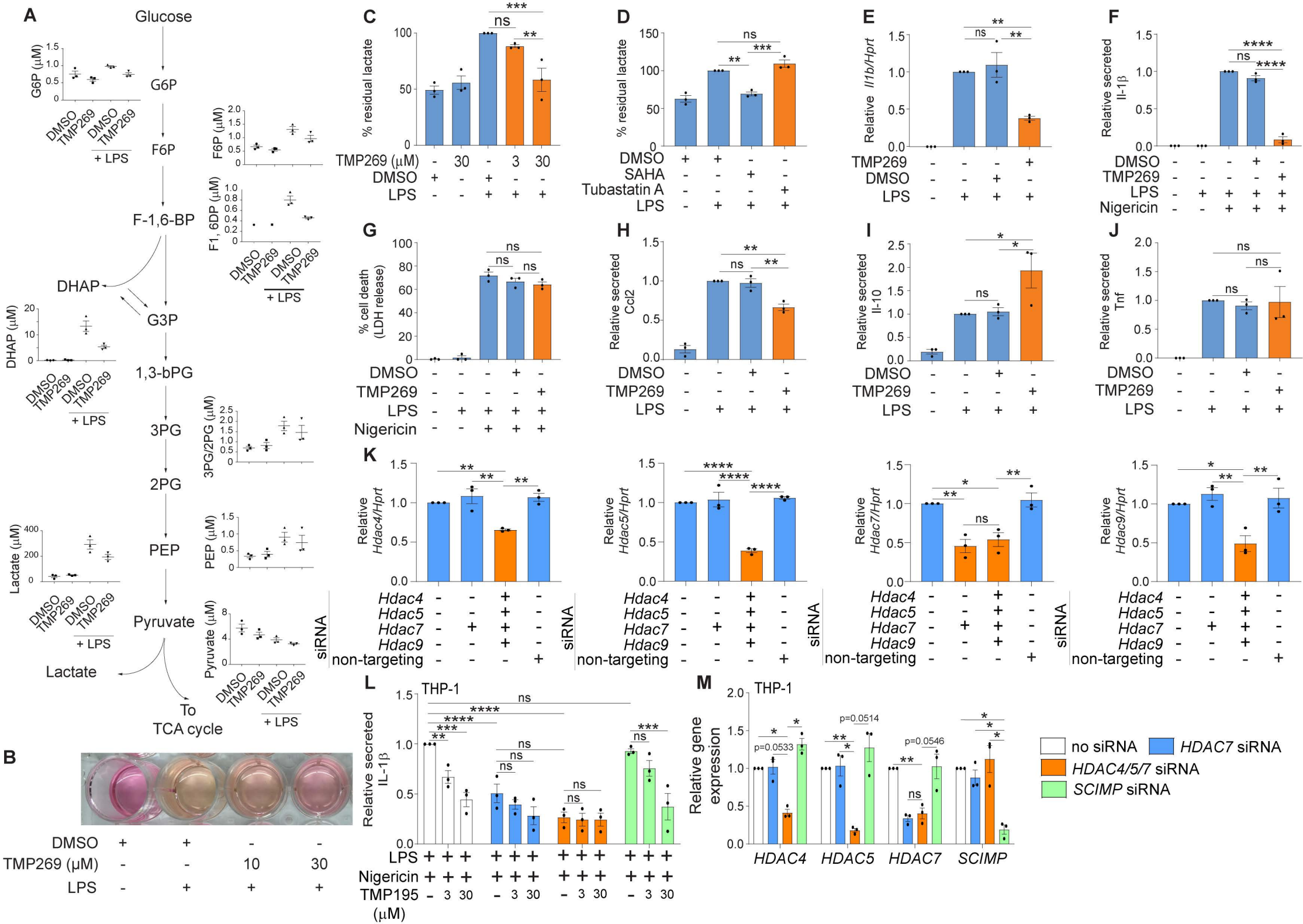
A
Glucose
G6P
F6P
F-1,6-BP
DHAP
G3P
1,3-bPG
3PG
2PG
PEP
Pyruvate
Lactate
To TCA cycle
G6P (μM)
F6P (μM)
F1, 6DP (μM)
DHAP (μM)
3PG/2PG (μM)
PEP (μM)
Pyruvate (μM)
Lactate (μM)
DMSO
TMP269
+ LPS
B
DMSO + + - -
TMP269 (μM) - - 10 30
LPS - + + +
C
% residual lactate
TMP269 (μM) - 30 - 3 30
DMSO + - + - -
LPS - - + + +
D
% residual lactate
DMSO + + - -
SAHA - - + -
Tubastatin A - - - +
LPS - + + +
E
Relative Il1b/Hprt
TMP269 - - - +
DMSO - - + -
LPS - + + +
F
Relative secreted Il-1β
DMSO - - - + -
TMP269 - - - - +
LPS - + + + +
Nigericin - - + + +
G
% cell death (LDH release)
DMSO - - - + -
TMP269 - - - - +
LPS - + + + +
Nigericin - - + + +
H
Relative secreted Ccl2
DMSO - - + -
TMP269 - - - +
LPS - + + +
I
Relative secreted Il-10
DMSO - - + -
TMP269 - - - +
LPS - + + +
J
Relative secreted Tnf
DMSO - - + -
TMP269 - - - +
LPS - + + +
K
Relative Hdac4/Hprt
Relative Hdac5/Hprt
Relative Hdac7/Hprt
Relative Hdac9/Hprt
siRNA
Hdac4 - - + -
Hdac5 - - + -
Hdac7 - + + -
Hdac9 - - + -
non-targeting - - - +
L
THP-1
Relative secreted IL-1β
LPS + + + + + + + + + + + +
Nigericin + + + + + + + + + + + +
TMP195 (μM) - 3 30 - 3 30 - 3 30 - 3 30
M
THP-1
Relative gene expression
p=0.0533
p=0.0514
p=0.0546
HDAC4
HDAC5
HDAC7
SCIMP
no siRNA
HDAC7 siRNA
HDAC4/5/7 siRNA
SCIMP siRNA

Supplementary Figure 6 – Related to Figure 6

(**A**) BMM were treated with DMSO, LPS+DMSO or LPS+TMP269 (30 μM) for 24 h. Intracellular concentrations of metabolites (μM) were determined by LC/MS.

(**B**) Colour change in the media of BMM following 24 h stimulation with LPS (100 ng/ml) in the presence of DMSO or TMP269 (10 or 30 μM).

(**C**) BMM were treated with TMP269 (3 or 30 μM) ± LPS (100 ng/ml) for 24 h, after which lactate concentrations in culture supernatants were determined.

(**D**) BMM were treated with LPS (100 ng/ml) in the presence of DMSO, SAHA (10 μM) or Tubastatin A (5 μM) for 24 h. Levels of secreted lactate were determined, and data are presented relative to the LPS treatment control.

(**E**) BMM were treated with LPS (100 ng/ml) ± DMSO or TMP269 (30 μM) for 4 h, after which mRNA levels of *Il1β* were determined by qPCR.

(**F**) BMM were primed with LPS (100 ng/ml) ± DMSO or TMP269 (30 μM) for 4 h, then treated with nigericin. Secreted IL-1β in supernatants was measured by ELISA.

(**G**) BMM were primed with LPS (100 ng/ml) for 4 h in the presence of DMSO or TMP269 (30 μM), then treated with nigericin. LDH release in culture supernatants was assessed by colorimetric assay.

(**H-J**) BMM were treated with LPS (100 ng/ml) ± DMSO or TMP269 (30 μM) for 24 h. Concentrations of Ccl2 (**H**), Il-10 (**I**) and Tnf (**J**) in culture supernatants were determined by ELISA.

(**K**) BMM were transfected with the indicated siRNAs. Total RNA was isolated and mRNA levels of *Hdac4*, *Hdac5*, *Hdac7* and *Hdac9* were determined by qPCR.

(**L-M**) PMA differentiated THP-1 were transfected with the indicated siRNAs and stimulated with LPS (100 ng/ml) for 4 h in the presence or absence of TMP195 (3 and 30 μM). Levels of secreted IL-1β (post-treatment with nigericin) in culture supernatants were measured by ELISA (**L**). Total RNA was isolated and mRNA levels of *HDAC4*, *HDAC5*, *HDAC7* and *SCIMP* were determined by qPCR (**M**).

All data in **A, C-M** (mean±SEM; n=3) are combined from three independent experiments (in **A**, F-1,6-BP levels in non-LPS-treated cells were below the level of detection in two of the three experiments). The image in **B** is from one experiment, and is representative of three experiments. Data in **C-E** and **H-J** are normalized to the LPS control, data in **F** are normalized to the LPS+nigericin control, data in **K, M** are normalized to the no siRNA control, while data in **L** are normalized to no siRNA LPS+nigericin control. Statistical significance for **C-K** was determined by one-way ANOVA and two-way ANOVA for **L** and **M** followed by Tukey's multiple comparison test (ns – not significant; * $p<0.05$; ** $p<0.01$; *** $p<0.001$; **** $p<0.0001$).

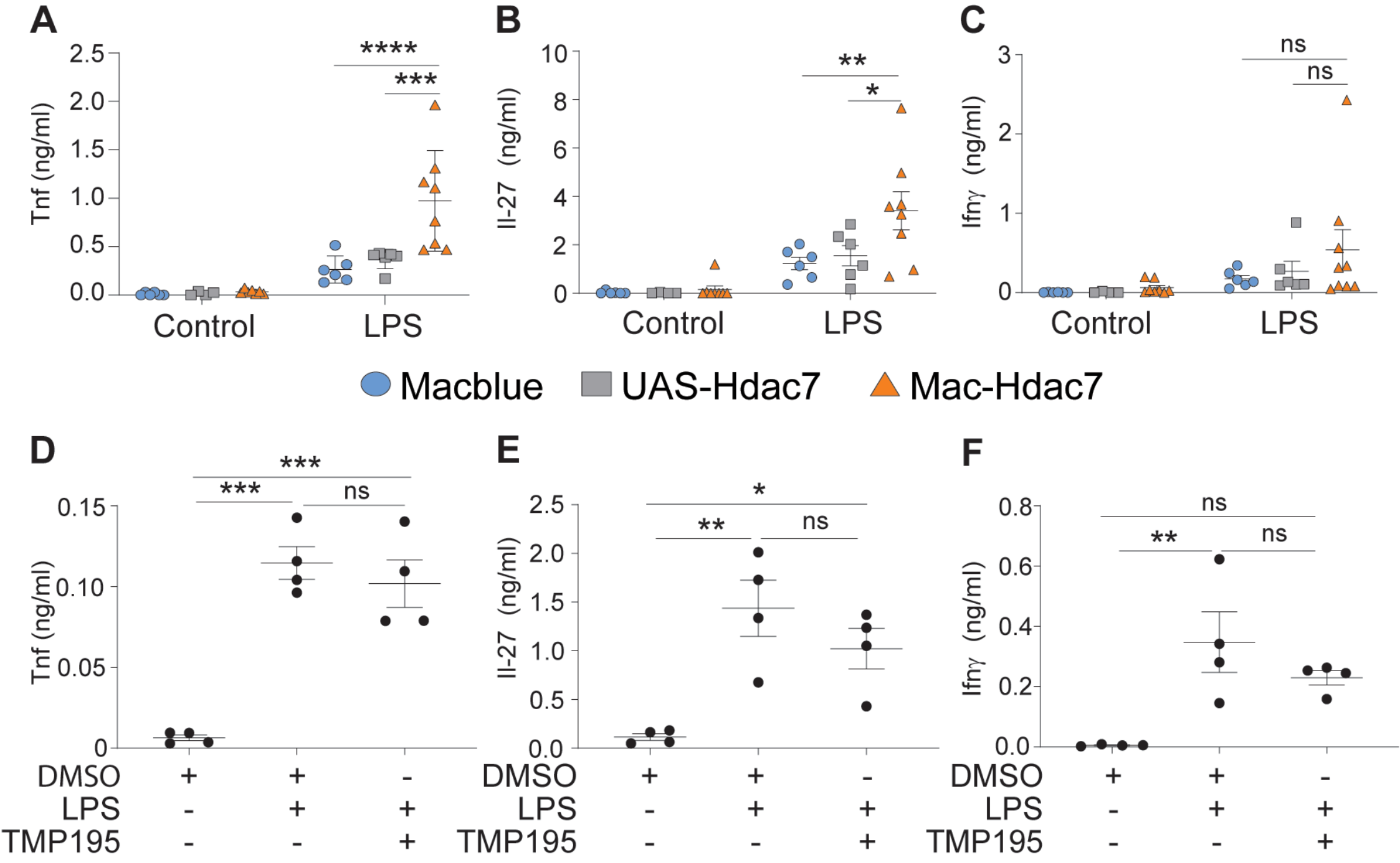
A
B
C
Tnf (ng/ml)
Il-27 (ng/ml)
Ifnγ (ng/ml)
Control
LPS
****
***
**
*
ns
Macblue
UAS-Hdac7
Mac-Hdac7
D
E
F
DMSO
LPS
TMP195

Supplementary Figure 7 – Related to Figure 7

(**A-C**) Mac-Hdac7 or littermate control (Macblue or UAS-Hdac7) mice were administered (i.p.) LPS (2 mg/kg) or an equivalent volume of PBS. Sera were collected 4 h post-LPS challenge, and levels of Tnf (**A**), Il-27 (**B**) and Ifnγ (**C**) were determined. Data are combined from two independent experiments (n=10-15 mice per group in total).

(**D-F**) C57BL/6J mice were administered (i.p.) DMSO or TMP195 (50 mg/kg), as well as PBS or LPS (2 mg/kg), as indicated. Sera were collected at 4 h post-LPS challenge, and levels of Tnf (**D**), Il-27 (**E**) and Ifnγ (**F**) were determined. Data shows mean+SEM of 4 mice per treatment group.

Statistical significance was determined by two-way ANOVA for **A-C** or one-way ANOVA for **D-F**, followed by Tukey's multiple comparison test (ns – not significant, * $p<0.05$; ** $p<0.01$; *** $p<0.001$; **** $p<0.0001$).

Supplementary Table 1 – Concentration of different metabolites in activated macrophages post TMP269 treatment – Related to Figure 6

Treatment	*3PG and 2PG*	*6PG*	*ACO*	*ACoA*	*ADP*	*AMP*	*ATP*
DMSO	0.6916	0.3617	0.2543	0.1183	10.6902	1.1415	45.2298
DMSO	0.5612	0.3691	0.1741	0.1434	7.1851	0.5386	35.0680
DMSO	0.8446	0.3858	0.1696	0.1656	6.6109	0.4731	41.3869
DMSO+LPS	2.2208	0.3790	0.3268	0.1452	9.1751	1.4396	39.7320
DMSO+LPS	1.4245	0.4749	0.5759	0.1255	5.6589	0.4173	36.7829
DMSO+LPS	1.7001	0.4379	0.2934	0.1275	5.8518	0.4974	30.5140
TMP269+LPS	2.1522	0.4111	0.2156	0.1094	7.4123	1.0344	33.6241
TMP269+LPS	1.0961	0.4655	0.3105	0.1167	4.8522	0.3334	31.9329
TMP269+LPS	1.1433	0.4079	0.1540	0.1199	5.0131	0.4091	29.8850

Treatment	*cAMP*	*CIT+ISO*	*CMP*	*CTP*	*DHAP*	*F16DP*	*F6P*
DMSO	0.0013	50.5565	1.0648	ND	0.1506	<0.31	0.7761
DMSO	0.0020	51.3928	0.5457	ND	0.0699	<0.31	0.5797
DMSO	0.0021	73.4730	0.5579	ND	0.1737	0.3251	0.6437
DMSO+LPS	0.0058	107.2689	0.9250	ND	17.2143	0.9519	1.4934
DMSO+LPS	0.0056	83.3348	0.6944	ND	12.1985	0.7435	1.2799
DMSO+LPS	0.0048	68.5565	0.6843	ND	10.5447	0.7094	1.1498
TMP269+LPS	0.0048	66.6666	0.6503	ND	6.4865	0.4823	1.2068
TMP269+LPS	0.0052	63.0629	0.4713	ND	4.9772	0.4249	0.8697
TMP269+LPS	0.0033	71.8968	0.6089	ND	4.3334	0.4632	0.8317

Treatment	*FUM*	*G1P*	*G6P*	*GA3P*	*GDP*	*GMP*	*GTP*
DMSO	1.4471	0.1696	0.9265	ND	4.2799	3.7023	ND
DMSO	1.2101	0.0958	0.6439	ND	3.0401	1.7795	ND
DMSO	1.1515	0.1352	0.6908	ND	2.7360	1.9861	ND
DMSO+LPS	0.9887	0.1819	1.0228	ND	3.3236	2.9889	ND
DMSO+LPS	0.9687	0.1502	0.9630	ND	1.9954	2.0513	ND
DMSO+LPS	1.0388	0.1688	0.9366	ND	2.3913	2.1686	ND
TMP269+LPS	0.9132	0.1844	0.8457	ND	2.8344	2.2916	ND
TMP269+LPS	0.8812	0.1100	0.6832	ND	2.0299	1.6099	ND
TMP269+LPS	0.7712	0.1082	0.6971	ND	2.0982	2.2509	ND

Treatment	*KGA*	*LAC*	*MAL*	*NAD*	*NADH*	*NADP*	*NADPH*
DMSO	1.6728	48.6466	3.7360	4.7125	0.2615	0.7356	ND
DMSO	0.9683	22.3454	3.3389	3.2991	0.0746	0.9267	ND
DMSO	1.0446	53.6139	3.2599	2.8540	0.0880	0.8038	ND
DMSO+LPS	0.9553	357.8036	3.8745	2.0912	1.0004	0.3893	ND
DMSO+LPS	0.4116	231.9181	3.2237	2.4187	0.8068	0.6667	ND
DMSO+LPS	0.5997	283.3560	3.1603	2.0743	0.8004	0.4798	ND
TMP269+LPS	1.0636	228.1533	2.6108	2.5416	0.6129	0.4500	ND
TMP269+LPS	0.7409	158.9479	2.2550	2.2928	0.7185	0.7849	ND
TMP269+LPS	0.6841	195.7581	1.7905	1.6038	0.3338	0.5589	ND

Treatment	*OAA*	*PEP*	*PYR*	*R5P*	*RL5P*	*SUC*	*UDP*
DMSO	ND	0.3568	6.9212	0.5664	0.2920	1.0256	2.4818
DMSO	ND	0.2488	4.8242	0.6272	0.2770	0.7853	1.9177
DMSO	ND	0.4106	5.5446	0.6566	0.3074	1.0603	1.8902
DMSO+LPS	ND	1.1915	3.6002	1.5228	0.7510	6.0142	3.2917
DMSO+LPS	ND	0.7057	4.5145	0.9303	0.4479	5.1016	1.2585
DMSO+LPS	ND	0.8242	3.4949	1.0275	0.5463	6.3203	2.1782
TMP269+LPS	ND	1.1844	3.3253	1.1176	0.5985	5.6443	3.1357
TMP269+LPS	ND	0.5076	3.4122	0.7277	0.3739	4.9878	1.3096
TMP269+LPS	ND	0.5375	3.0272	0.7825	0.3850	5.2126	2.0144

Treatment	*UMP*	*UTP*
DMSO	0.9497	9.3420
DMSO	0.3489	10.6394
DMSO	0.3912	11.4723
DMSO+LPS	0.7205	11.0945
DMSO+LPS	0.3841	8.6267
DMSO+LPS	0.4700	12.9095
TMP269+LPS	0.6917	11.8250
TMP269+LPS	0.2818	10.2206
TMP269+LPS	0.5129	11.9935

**ND – Not detected

Supplementary Table 2 – List of oligonucleotides used in this study – Related to STAR METHODS

A – List of qPCR primers:

Species	Gene	Forward Primer (5'-3')	Reverse Primer (5'-3')
Mouse	*Ccl2*	CCCACTCACCTGCTGCTACTCA	GCTTCTTTGGGACACCTGCTG
Mouse	*Il10*	GGTTGCCAAGCCTTATCGGA	ACCTGCTCCACTGCCTTGCT
Mouse	*Il12b*	GGAAGCACGGCAGCAGAATA	AACTTGAGGGAGAAGTAGGAAT
Mouse	*Nos2*	CAGCTGGGCTGTACAAACCTT	CATTGGAAGTGAAGCGTTTCG
Mouse	*Hdac4*	GCTCTCCCAGCTCTCCAGCA	GTTGTGAGCTGCTGCACCGT
Mouse	*Hdac5*	TGAGAGGCAGGCCCTTCAGT	CCTCCAGTGCCACTCCCAAC
Mouse	*Hdac9*	TGGAGCAGCAGAGGCAAGAA	TTGCCACTGCCCTTTCTCGT
Mouse	*Ctbp1*	GTGCCCTGATGTACCATACCA	GCCAATTCGGACGATGATTCTA
Mouse	*Hprt*	GCAGTACAGCCCCAAAATGG	AACAAAGTCTGGCCTGTATCCA
Human	*HDAC4*	GGTTTGAGAGCAGGCAGAAC	CAGAGAATGAGGCCAAGGAG
Human	*HDAC5*	ATGTATGCTGTGCTGCCTTG	GTAGGAGTTTTGCGGTGATG
Human	*HDAC10*	GTTGGGATGGGAAAGCTG	TCAAATCCTGCCGAGACCA
Human	*SCIMP* (control gene)	TACTTTCACAGTTCAGGATTC	ACAGACACAGTACAGGATGAG
Human	*HPRT*	TCAGGCAGTATAATCCAAAGAT	AGTCTGGCTTATATCCAACACT

B – List of siRNA used

Species	Gene	si-RNA sequences
Mouse	*Hdac4*	#1-GGUUAUGCCUAUCGCAAAU
		#2-GUGGAUAGCGACACCAUAU
		#3-GAAAUUACGCUCAAGGCUU
		#4-CAACAUGGCUUUCACGGGU
Mouse	*Hdac5*	#1-UGACAGCCGUGAUGACUUU
		#2-GCAUGAGGACGGUGGGUAA
		#3-UCGAAAGGAUGGCACUGUU
		#4-UAGAGAAAGUCAUCCGAGAU
Mouse	*Hdac9*	#1-GCUCCAGGAUUUGUAAUUA
		#2-CCACAGCAGCGCAUACUAA
		#3-CAAGAUAGCAAGGAUGAUU
		#4-GCAGAAUCCUCGGUCAGUA
Human	*HDAC4*	#1-UCGUGUAUGACACGCUGAUGCUGAA
		#2-CAGAGCGGAGUGUCGACCUCCUAUA
		#3-CCACCGGAAUCUGAACCACUGCAUU
Human	*HDAC5*	#1-CAUUGCCCACGAGUUCUCACCUGAU
		#2-CAGAAACAGCAUGACCACCUGACAA
		#3-CAAGUUCAUGAGCACAUCCUCUAUU
Human	*HDAC10*	#1- CGGAGUCAGUGUGCAUGACAGUAC
		#2- UCACUGCACUUGGGAAGCUCCUGUA
		#3- GGUGGUUUCCUGAGCUGCAUCUUGG
Human	*SCIMP* (control gene)	#1- GAAACACAAGCAAGUAGAUGAAGA
		#2- CCGCUACAUACUCACUGGUAAAUAA
		#3-UCUUAAUGAGUCGCCAGUUCAAUUA